KIF7 deletion in a mouse model of human ciliopathy alters cerebral cortex development

Maria Pedraza[1,#], Valentina Grampa[1], Julien Puech[1], Sophie Scotto-Lomassese[1], Aude Muzerelle[1], Aska Mohammad[1], Nicolas Renier[2], Christine Métin[1,§] and Justine Masson[1,§,*]

1. INSERM, UMR-S1270, Institut du Fer à Moulin, Sorbonne Université.
2. Institut du Cerveau et de la Moelle Épinière, Laboratoire de Plasticité Structurale, Sorbonne Université, INSERM U1127, CNRS UMR7225, 75013, Paris, France.

* Correspondence to justine.masson@inserm.fr
[&] These authors contributed equally to this work
[#] Present address: Department of Neurology. Hospital, Clínico Universitario de Valladolid, Valladolid, Spain.

CM and JM conceptualized the project and supervised the work. MP, VG, JP, SC, AM AM, NR, CM and JM perfomed experiments. MP, VP, NR, CM and JM analyzed the data. MP, JM and CM wrote the paper.

Running title: Kif7 deletion and cortical development

Keywords: kinesin, Sonic Hedghog pathway, mouse model, embryonic development, cortical projections, interneuron migration

ABSTRACT

Mutations of KIF7, a key ciliary component of the Sonic hedgehog (SHH) pathway, are associated in humans with malformations of the cerebral cortex and clinical features suggestive of cortical dysfunction. In both humans and mice, KIF7 regulates the processing of GLI-A and GLI3-R transcription factors in a SHH-dependent manner. To understand the pathological mechanisms involved in cerebral cortex defects, we took advantage of a *Kif7* −/− mouse model in which the cellular mechanisms leading to the corpus callosum agenesis had already been investigated (Putoux et al, 2019). We observed a stronger impact of the *Kif7* deletion on the development of the mouse dorsal cortex, in agreement with the important role of GLI3-R in the pattering of the dorsal telencephalon. The intermediate progenitor layer and cortical plate no longer segregated, preventing the formation of the intermediate zone, and subplate cells were missing. Corticofugal axons did not develop properly leading to a delayed colonization of the telencephalon by thalamo-cortical axons. These structural defects altered the cortical distribution of GABAergic interneurons generated in the basal telencephalon, which moreover exhibited intrinsic migration defects resembling those of control interneurons treated with cyclopamine. These migratory defaults suggested that the SHH pathway can no longer be activated in cortical interneurons generated in the ventral telencephalon of *Kif7* -/- mice.

INTRODUCTION

The primary cilium is a tiny microtubule-based organelle present on the surface of nearly all mammalian cell types including neurons, which functions as a signaling hub and transduces several signaling pathways comprising SHH, Wnt, Delta/Notch and mTOR pathways (Park et al., 2019). Primary cilium dysfunction causes pleiotropiques diseases named ciliopathies. KIF7 is a ciliary kinesin responsible for the trafficking and the positive and negative regulation of the GLI transcription factors in the primary cilium of mammals (Haycraft et al., 2005). Loss of function of KIF7 in the mouse has shown that *Kif7* regulates Sonic Hedghog (SHH) signalling by acting downstream of Smoothened and upstream of GLI2 and Gli3 (Cheung et al., 2009; Endoh-Yamagami et al., 2009; Liem et al., 2009) see review in (Ingham and McMahon, 2009; Pedersen and Akhmanova, 2014). Studies in mice moreover established that KIF7 activity is dependent on the expression level of SHH. In the absence of SHH, KIF7 localizes to the base of the primary cilium (Liem et al., 2009). GLIs factors are phosphorylated and addressed to the proteasome at the base of the primary cilium for degradation, leading to the formation of a cleaved and stable transcriptional repressor (GLI3-R). In the presence of SHH, KIF7 accumulates at the distal tip of the primary cilium (Endoh-Yamagami et al., 2009; Liem et al., 2009) and associates with full length GLI2/3 which are converted there in transcriptional activators (GLI-A, (Han et al., 2019)). Since 2011, ten studies have identified patients carrying mutations in the *KIF7* gene. *KIF7* mutations were responsible of ciliopathies classified according to clinical features as hydrolethalus, acrocallosal, Joubert and Greig cephalopolysyndactyly syndromes (al-Gazali and Bakalinova, 1998; Ali et al., 2012; Putoux et al., 2012, 2019; Walsh et al., 2013; Barakeh et al., 2015; Ibisler et al., 2015; Tunovic et al., 2015; Asadollahi et al., 2018; Niceta et al., 2020). MRI investigations revealed macrocephaly, ventricles enlargement, and corpus callosum alterations. They also showed the characteristic hindbrain abnormalities observed in most ciliopathies such as molar tooth sign (MTS) and cerebellar atrophy. Patients displayed neurodevelopmental delay, intellectual disability and seizure (Dafinger et al., 2011; Ali et al., 2012; Putoux et al., 2012; Ibisler et al., 2015) and the mild but frequent cortical malformations described in these patients lead to postulate that they present cortical dysfunction.

In physiological condition, the proper activity of the cortex relies on the excitatory/inhibitory balance i.e. on the ratio, positioning and connectivity of excitatory glutamatergic and inhibitory GABAergic neurons, generated from progenitors in the dorsal and ventral forebrain, respectively. The cortical neurons of dorsal and ventral origin each migrate to the developing cortex, the so-called cortical plate (CP), according to a specific timeline allowing the establishment of proper connections in the CP. SHH plays a central role in establishing the dorso-ventral patterning of the forebrain, and in regulating the proliferation and differentiation of cortical progenitors of dorsal and ventral origins. At early embryonic stage, the ventral expression of SHH orchestrates the ventro-dorsal (Chiang et al., 1996; Shimamura and Rubenstein, 1997) and medio-lateral (Kohtz et al., 1998) regionalization of the mouse forebrain and the differentiation of ventral cell types (Chiang et al., 1996). Shh ablation performed after forebrain patterning alters the specification of distinct subgroups of GABAergic interneurons (Machold et al., 2003; Xu et al., 2005, 2010), likely in response to differential SHH expression levels in subregions of the ventral telencephalon (Sousa and Fishell, 2010). Interestingly, conditional ablation of Shh and Smoothened (Smo) in the embryonic cortex reduces the proliferation of dorsal progenitors (Komada et al., 2008), demonstrating a minimal Shh expression in the dorsal telencephalon, even before birth (Dahmane et al., 2001). Beside its role on proliferation and specification, SHH also controls

the migration of interneurons to the cortical plate (Baudoin et al., 2012; Higginbotham et al., 2012; Komada, 2012; Komada et al., 2013; Hasenpusch-Theil and Theil, 2021).
In the embryonic telencephalon, GLIs transcription factors mediate SHH signals in complex and specific ways. The three GLI factors identified in mammals are expressed in the mouse forebrain: GLI1 along the source of SHH in the ganglionic sulcus, and GLI2 and GLI3 at a progressive distance of the SHH source, more dorsally (Hui et al., 1994; Yu et al., 2009; Sousa and Fishell, 2010). GLI1 acts uniquely as a pathway activateur whereas GLI2 and GLI3 can be processed in transcriptional activators or inhibitors in the primary cilium. However, both GLI1 and GLI2 function primarily as transcriptional activator in the ventral forebrain (Yu et al., 2009). GLI1 and GLI2 mutants show mild phenotypes (Park et al., 2000; Bai and Joyner, 2001) and GLI2 seems required to transduce high level SHH signals in mice (Ding et al., 1998). In contrast, the development of the dorsal cortex where principal excitatory neurons differentiate mainly depends on the expression of the GLI3-R repressor (Tole et al., 2000; Rallu et al., 2002). Following patterning, Gli3R/A ratio is critical for specifying the fate of cortical progenitors and regulating cell cycle kinetics (Wang et al., 2011; Wilson et al., 2012).

Given the crucial role of KIF7 in regulating the GLIs pathways and given the important role of Gli3-R and GLIs2/3-A in regulating the early developmental stages of the dorsal and ventral telencephalon, respectively, we examined here the cortical development, the establishment of long distance projections with the thalamus and the migration of GABAergic interneurons (cIN) in *Kif7* -/- mice at embryonic stage E14.5, a key period in corticogenesis when the cortical plate begins to form and cIN start to invade the developing cortex. Previous studies investigated the mechanisms underlying corpus callosum agenesis in patients with *KIF7* mutation using *Kif7* KO (*Kif7* -/-) mice (Putoux et al., 2019). Although cortical neurogenesis defect were observed in principal cells electroporated with Kif7 shRNA (Guo et al., 2015), the Influence on the cortical cytoarchitecture of developmental abnormalities associated with ciliopathies is poorly understood. Here, we further investigated the influence of abnormal SHH signaling in *Kif7* -/- mice on the migratory behavior of cIN, by recording living cortical slices from *Kif7* -/- mice and from control mice treated with pharmacological activator and inhibitor of the SHH pathway. We moreover determined the local distribution of the SHH protein in the embryonic cortex.
Developmental defects leading to permanently displaced neurons, abnormal formation of cortical layers and defective cortical circuits could be responsible of epilepsy and/or intellectual deficiency described in KIF7 patients.

RESULTS

Kif7 knock-out mice as a model to investigate the structural cortical defects that could lead to clinical feature in patients carrying KIF7 mutation.

The *KIF7* gene is located on chromosome 15 in human and encodes a 1343 aa protein containing in the N-terminal part a kinesin motor domain and a GLI-binding domain, followed by a Coiled-coil region and in the C-terminal part, a Cargo domain able to bind a diverse set of cargos (Maurya et al., 2013). The Table 1 summarizes the clinical features associated with mutations targeting either the kinesin or GLI binding domain in the N-terminal part of the protein, the Coiled-coil domain or the N-terminal Cargo domain. Interestingly, various mutations associated with the same clinical picture, suggesting that KIF7 mutations, whatever their nature, could lead to protein loss of function, for example by altering the protein structure and solubility as proposed by (Klejnot and Kozielski, 2012). All patients carrying

mutation in the *KIF7* gene have developpemental delay (DD) and intellectual deficit (ID) associated with classical defects of ciliopathies such as ventricle enlargement, macrocephaly, corpus callosum (CC) agenesis and molar tooth sign (MTS). Some patients have anatomical cerebral cortex defects as poor frontal development, atrophy, pachygyria and heterotopia (al-Gazali and Bakalinova, 1998; Putoux et al., 2011; Walsh et al., 2013; Tunovic et al., 2015) that could participate not only to DD and ID but moreover to seizure as observed in a quarter of all patients. In this context, we used a murine model in which the *Kif7* gene had been deleted (*Kif7* -/-) (Cheung et al., 2009) to investigate the consequence of KIF7 loss of function on the cortex development. *Kif7* -/- mice have been previoulsy characterized as dying at birth with severe malformations, including exencephaly in a third of the mutants, skeletal abnormalities (digits and ribs), neural tube patterning defects, microphtalmia, absence of olfactory bulbs and CC agenesis (Cheung et al., 2009; Endoh-Yamagami et al., 2009; Putoux et al., 2019). In the present study, we studied the Kif7 mutation in a mouse strain with a mixed genetic background in which exencephaly at E14.5 was observed at the same frequency in *Kif7 -/-* and control embryos. As previously reported, E14.5 *Kif7 -/-* embryos displayed microphtalmia (Fig.1A, black arrow) and polydactily (not illustrated). Interestingly, skin laxity previously reported in ciliopathic patients (Walczak-Sztulpa et al., 2010; Chen et al., 2015) was observed in all mutants (Fig.1A, white arrow). Comparison of brains from *Kif7* -/- embryos and control littermates at E14.5 revealed that *Kif7* mutants could be distinguished by the absence of olfactory bulbs (Fig.1B, white arrows), a prominent diencephalon and a thinning of the dorsal cortex allowing the lateral ventricles to be seen through (Fig.1B, black arrow).

<u>*Kif7* invalidation alters the development of the cortex at E14.5.</u>

Analyses performed on rostro-caudal series of frontal sections (Fig.1C1) confirmed that the brain of *Kif7 -/-* embryos exhibited at E14.5 enlarged lateral ventricles (Fig.1C2) and thinned dorsal cortex (Fig.1C3) resulting however in unchanged total width and height of the telencephalon (Fig.1C4,5). KIF7 depletion in E10.5-E11.5 mouse embryos was reported to alter the dorso-ventral patterning of the medial forebrain (Putoux et al., 2019), accordingly with the decreased expression of the transcriptional repressor GLI3R (Cheung et al., 2009; Endoh-Yamagami et al., 2009). GLI3 loss of function (Fotaki et al., 2006; Magnani et al., 2010) has been associated with an abnormal dorso-ventral patterning of the telencephalon. Here, we confirmed the decreased expression of GLI3R in the cortex of KIf7 -/- embryos (Fig.S1). However, the frontier of expression of GSH2 (Fig.1D1) and TBR2 (Fig.1D2), two transcription factors respectively expressed in the ventral and dorsal telencephalon, was preserved in the pallium-subpallium boundary (PSB) at E14.5 in *Kif7* -/- embryos suggesting a rather normal dorso-ventral patterning of the telencephalic vesicles in their lateral side.

The thinning of the dorsal cortex of *Kif7* -/- embryos at E14.5 convinced us to examine the structural organization of the cortex of *Kif7* -/- embryos. At E14.5, the mouse cortex can be described as a stack of three specialized domains: i) the upper/superficial cortical layers containing post-mitotic cells generated in the proliferative zones of the cortex, including TBR1(+) post-mitotic neurons located in the cortical plate (CP); ii) the deep proliferative layers, ventricular and subventricular zones (VZ and SVZ, respectively), located along the lateral ventricle; iii) the intermediate zone (IZ) located between the CP and the proliferative layers, which hosts the radially and tangentially migrating neurons and growing axons. In control embryos, TBR1(+) cells formed a rather regular, radially organized CP surrounded by two thin continuous layers of MAP2(+) neurons located respectively in the upper marginal zone (MZ) and the bottom subplate (SP) (Fig.2A, left). In *Kif7 -/-* embryos, the TBR1(+) CP cells

appeared more clustered and the thickness of the upper MAP2(+) layer was extremly irregular. MAP2(+) cells were no longer observed below the CP in the dorsal cortex (Fig.2A, arrow on right panel). Moreover, focal heterotopia characterized by an abnormal accumulation of TBR2(+) cells were observed in the dorsal or lateral cortex of *Kif7* -/- embryos, either at the ventricular or pial surface (Fig.S2). TBR2 labels the intermediate progenitors (IP) of principal cells, which normally form a dense layer in the SVZ of the cortex (Fig.2B1, left). Beside sporadic heterotopia, the TBR2(+) layer constantly showed an abnormal positioning in the dorsal cortex of *Kif7* -/- embryos. TBR2(+) cells indeed reached the brain surface (Fig.2B1, arrow) where they mixed up with post-mitotic TBR1(+) cells instead of keeping a minimal distance with TBR1 cells as observed in control brains (Fig.2B2, arrow) and in the lateral cortex of *Kif7* -/- brains (Fig.2B2). Therefore, intermediate progenitors and post-mitotic neurons no longer segregated in the dorsal cortex of *Kif7* -/- embryos and no IZ was observed (Fig.2B2, white arrow).

<u>The loss of *Kif7* alters the connectivity between the cortex and the thalamus at E14.5</u>

The intermediate zone (IZ) hosts the radially and tangentially migrating neurons and comprises by the growing cortical and thalamic projections (Price et al., 2006). Corticofugal axons develop from early stages: the trailing process of post-mitotic neurons migrating radially to the CP first elongates tangentially in the IZ and then differentiates as an axon (Hatanaka and Yamauchi, 2013; Kon et al., 2017). We thus examined whether the defaults observed in the CP and the lack of IZ in the dorsal cortex of *Kif7* -/- embryos did associate with developmental abnormalities of the corticofugal projection. We labeled corticofugal axons by inserting small crystals of DiI in the dorsal or lateral cortex in E14.5 paraformaldehyde fixed brains. After DiI had diffused along corticofugal axons, we analyzed labeled axons on coronal sections. In both control and *Kif7* -/- brains, CP neurons located in the dorsal or lateral cortex extended axons below the CP toward the PSB (Fig.3A). DiI injections in the dorsal cortex of control and *Kif7* -/- brains labeled much less axons than injections in the lateral cortex, according to the latero-medial gradient of cortical development (Fig.5A3). Very remarkably, the cortical bundles labeled from similar cortical regions were always much smaller in *Kif7* -/- than in wild type brains (Fig.3A, compare right and left columns). Whereas dorsal injections labeled large bundles crossing the PSB in control brains, only a few axons reached the PSB in *Kif7* -/- brains, showing that corticofugal axons growth was severely hampered in the dorsal cortex of *Kif7* -/- embryos. Corticofugal axons labeled from lateral injection sites in control brains crossed the PSB, extended within the embryonic striatum and continued medially in the internal capsule (IC) where they met thalamic axons retrogradely labeled from the lateral cortex (Fig.3A3, left panel). In *Kif7* -/- embryos, lateral injections labeled axons that either spread in the striatum (Fig. 3A3, right panel) or extended ventrally to the cerebral peduncle (Fig.3A3, right panel, white arrow), a trajectory never observed in control brains. Moreover, no thalamic axons were retrogradely labeled from the lateral cortex. To identify the trajectory of thalamic axons in *Kif7* -/- embryos, we immunostained coronal sections of E14.5 brains with antibodies against the Netrin G1a (NG1a), an early marker of thalamocortical axons [TCA, (Braisted et al., 2000)]. At E14.5, in both control and *Kif7* -/- brains, NG1a antibodies labeled a large population of dorsal thalamic neurons (Fig.3B, Fig.S3A). In control brains, thalamic axons made a right angle turn to join the IC.Then they extended to the PSB and some axons entered the lateral cortex (Fig.3B, left panel and Fig.3C). In *Kif7* -/- embryos, most thalamic axons stopped their course at the exit of the diencephalon while some of them formed a short and thick bundle oriented ventrally to the surface of the basal telencephalon (Fig.3B, right panel, white arrow). No evident structural defect could be observed at the telo-diencephalic junction (Fig.S3B). Given the complexity of the trajectory of NG1a

thalamic axons, we immunostained thalamic axons in whole brains and imaged them after transparisation using a light-sheet microscope. Reconstruction and three-dimension analysis of labeled projections confirmed that thalamic axons made a sharp turn to reach the IC and then navigated straight to the PBS in control brains (Fig.3C and S3B). In contrast, most thalamic axons stopped their course after leaving the diencephalon in *Kif7* -/- embryos, and formed two large bundles, one oriented to the IC (Fig.3C,white star) and another one oriented caudally (Fig.3C, white arrow). This last projection was never observed in control brains. The present analysis identified impaired trajectories of corticofugal and thalamo-cortical projections at E14.5 in the basal forebrain of *Kif7* -/- animals, suggesting impaired axonal guidance mechanisms in the basal forebrain. Because cortical interneurons (cIN) are born in the basal forebrain and likely depend for the first stages of their migration on contact/functional interactions with pioneer corticofugal projections (Métin and Godement, 1996; Denaxa et al., 2001), we also examined the distribution of cIN in the developing cortex of *Kif7* -/- animals.

<u>*Kif7* invalidation alters the cortical distribution of cIN at E14.5.</u>

Cortical interneurons are generated outside of the cortex, in the medial and caudal ganglonic eminences (MGE, CGE) and preotic area (POA) of the ventral forebrain. They enter the lateral cortex at E12.5 - E13.5, depending on strains, and colonize the whole cortex by organizing two main tangential migratory streams, a superficial one in the MZ, and a deep and large one in the lower IZ/SVZ (Tanaka et al., 2003; Yokota et al., 2007). Intermediate cortical progenitors of the SVZ and meninges strongly express *CxCl12* mRNA (Tiveron et al., 2006), coding for a chemokine essential for cIN to recognize their tangential pathways of migration in the developing cortex. CXCL12 promotes the tangential progression of cIN and prevents the migration switch from a tangential to a radial mode required for cIN to colonize the CP (Stumm et al., 2003; Tiveron et al., 2006; Li et al., 2008). We analyzed the expression of *CxCl12* mRNA in the cortex of mutant embryos using in situ hybridization experiments at E14.5, a stage when TBR2(+) SVZ cells show defective positioning of in the dorsal cortex of *Kif7* -/- embryos. In control brains, *CxCl12* mRNA showed a latero-medial gradient of expression in the SVZ, which ended at the frontier with the hippocampus. In contrast, *CxCl12* mRNA was no longer expressed in the dorsal cortex of *Kif7* -/- embryos (Fig.4A, black arrow), in the region where TBR2(+) cells starts to position at the brain surface (Fig.4B1). We thereafter analyzed the cortical distribution of tomato(+) MGE-derived cIN at E14.5 in control Nkx2.1-Cre, Rosa26-TdTomato transgenic embryos and in *Kif7* -/- , Nkx2.1-Cre, Rosa26-TdTomato transgenic mutant embryos (Fig.4B and see methods). The latero-medial extent of both the superficial and deep tangential migratory streams was significantly shortened in *Kif7* -/- brains as compared to control brains (Fig. 4B1, white arrows). Very remarkably, the cIN deep tangential stream stopped in the region where the layer of TBR2(+) cells started its abnormal switch to the surface of the cortex (Fig.4B1, arrow) and did not colonize the dorsal cortex (Fig.4CB2). In addition to an abnormal latero-dorsal extension, cIN presented an altered radial distribution in the cortex of *Kif7 -/-* embryos (Fig.4C). The superficial migratory stream was thinner and denser in the MZ of *Kif7 -/-* embryos as compared to control (Fig.4C1) and the distance between the superficial and deep tangential migratory streams was significantly diminished in the lateral cortex of *Kif7* -/- mutants (Fig.4C2). This decrease is in agreement with the reduced corticofugal projections identified in *Kif7* -/- mutants. The reduced latero-dorsal distribution of cIN and their abnormal distribution in the cortical thickness reflected structural and molecular abnormalities identified in the cortex of *Kif7* -/- embryos. To verify if migratory defaults proper to *Kif7* -/- cIN could moreover

contribute to their abnormal distribution in the cortex of *Kif7* -/- embryos, we analyzed the migration of cIN in living cortical slices.

<u>*Kif7* deletion and SHH pathway activity both affect the migratory behavior of cIN in cortical slices.</u>

The forebrain of E14.5 Nkx2.1-Cre;Rosa26-TdTomato transgenic embryos exhibiting or not a *Kif7* deletion (control and *Kif7* -/-, respectively) were sliced coronally to image the cortical migration of cIN by time-lapse video-microscopy (Fig.5). In control slices (Fig.5A), fluorescent cIN migrated tangentially from the PSB to the dorsal cortex in two main pathways, a superficial one in the MZ and a deep one in the lower IZ/SVZ. All along these pathways, some cIN operated a tangential to oblique/radial migration switch to colonize the CP. High cell density in the MZ prevented a dynamic analyze of migrating cells. In the deep tangential stream, a large proportion of cells imaged at the start of the recording session (59.3 %), either maintained tangentially oriented trajectories in the deep stream (28.7 %, red trajectories in Fig.5A, left column of Fig.5B), or reoriented to the CP along oblique (and less frequently radial) trajectories (30.6 % green trajectories in Fig.5A, left column in Fig.5B). A majority of cells reached the CP surface and remained there. A smaller proportion of cIN moved from the deep stream to the opposite - ventricular- side of the slice (12%, blue trajectories in Fig.5A, left column in Fig.5B). In the VZ, deep stream, and CP, a minimal proportion of cIN (3.6 %) moved very short distances or remained immobile (dark colors in the left column of Fig.5B). A significant proportion of cIN (15.6 %) migrated radially, traveling all over the cortex thickness and frequently inverting their polarity in the MZ or at the ventricular surface (pink trajectories in fig.5A, left column in Fig. 5B). Finally, 8 % (orange) of the recorded cIN moved backward to the ventral brain and 1.7 % of them (grey) did not show any specific directionality and layer specificity and were classsified as chaotic (Fig.5A, left column in Fig.5B). A large majority of cIN presented a characteristic saltatory behavior, alternating stops and fast moves (Bellion, 2005) Analyses of resting and moving phases of the largest cIN population recorded in the deep stream and/or moving to the CP is illustrated in Fig.5D1-3 (left column of histograms). To our surprise, the trajectories followed by cIN in the cortical slices of *Kif7* -/- embryos dramatically differed from those in control slices (Fig.5B and scheme in Fig.5C, *Kif7* -/-). The number of cIN migrating tangentially in the deep migratory stream and moving to the CP from the deep stream dropped drastically (17.8 % as compared to 59.3 % in control slices), at the benefit of immobile cIN (35.7 % as compared to 3.6 % in control slices). Immobile cIN were particularly numerous in the SVZ/lower IZ. Almost the same proportion of cIN moved to the ventricle and to the CP (10.2 % and 13.9 %, respectively, as compared to 11.7 % and 30.6 % in control slices) suggesting that the radial asymmetry of cortical slice was lost for *Kif7* -/- cIN. The proportion of cIN migrating radially across cortical layers remained similar as in control slices (17.2 % versus 15.6 % in control) but the proportion of cIN with chaotic trajectories strongly increased (7.8 % versus 1.7 % in control slices, Fig.5B, second column). Another major change observed in the *Kif7* -/- cortical slices was a significant decrease of the migration speed (excluding immobile cIN) (Fig.5D1) and an abnormal saltatory behavior, with less frequent but longer resting phases than in control slices (Fig.5D2,D3). Trajectories were analyzed at E14.5 in the lateral and latero-dorsal cortex that expresses CxCl12 mRNA in both control and *Kif7* -/- embryos (Fig.5A). Because CXCL12 is a potent chemoattractant for migrating cIN, the very large proportion of immobile cIN recorded in the CXCL12-expressing deep stream of *Kif7* -/- slices was suggestive of intrinsic migratory defaults of *Kif7* -/- cIN. Kif7 ablation has been shown to induce either transcriptional SHH signaling activation by inhibiting the processing of GLI3 in GLI3-R repressor, or transcriptional SHH

signaling inhibition by inhibiting the positive impact of KIF7 on the GLI1/2 dependent SHH signaling (Cheung et al., 2009). We thus examined whether the acute application of drugs able to either promote or inhibit the SHH signaling could induce in wild type cIN migratory defaults resembling those of cIN in *Kif7* -/- cortical slices. SHH application on control slices minimaly affected the trajectories of cIN (Fig.5B, compare left and right columns), except an increased proportion of cIN migrating radially (29 % compared to 15.6 % in control slices) at the expense of cIN migrating from the deep stream to the CP (20.8 % instead of 30.6 % in control slices). In addition, cIN moving radially across the cortical layers no longer stopped in the CP and frequently moved backward to the VZ (Fig.5B,C). The frequency of atypical trajectories (grey, Fig.5B) did not increase, and the migration speed of cIN was slightly decreased compared to control slices (Fig.4D1). The main dynamic alteration of SHH treated cIN was the increased duration of resting phases (Fig.5D2,D3). On the contrary, application of the SHH pathway inhibitor cyclopamine strongly altered cIN trajectories. For example, the proportion of immobile cIN and of cIN moving short distance reached 33.7 % as compared to 3.6 % in control slices (Fig.5B). Most immobile cells in cyclopamine treated slices were located in the deep stream, and only few cIN switched from the deep stream to the CP at the benefit of cIN with aberrant trajectories, directed to the lateral cortex. Therefore, inhibiting the SHH pathway mainly affected the ability of cIN to move tangentially in the deep stream and to switch to the CP (Fig.5C), as previously observed in *Kif7* -/- slices. Globally, cIN trajectories in cyclopamine treated slices recalled the trajectories of cIN in *Kif7* -/- cIN (Fig.5B, compare columns 2 and 3), suggesting that *Kif7* ablation resembled the cyclopamine-mediated SHH pathway inhibition. Nevertheless, whereas the migration speed of *Kif7* -/- cIN was significantly decreased in the deep tangential pathwaybut not in CP, cyclopamine application decreased the migration speed only in CP (Fig. 5D). The strong influence of cyclopamine on the cortical migration of cIN led us to determine the distribution of the endogenous activator - SHH - of the SHH pathway in the developing cortex.

Distribution of *Shh* mRNA and SHH protein in the E14.5 cortex

Shh mRNA is strongly expressed by the mantle zone of the ganglionic eminences (MGE, CGE) and POA during the time cIN differenciate (Xu et al., 2005; Kon et al., 2017) but its level of expression in cIN after they reach the cortex is controversial (Sahara et al., 2007; Baudoin et al., 2012; Komada, 2012). We thus reexamined *Shh* mRNA expression in forebrain and SHH protein distribution in cortical layers.

In situ hybridization (ISH) experiments performed at E13-E15.5 confirmed the strong expression of *Shh* mRNA in the ventral forebrain, especially in the SVZ and mantle zone of the MGE (Fig.A1,B1) in aggrement with Shh-dependent *Gli1* mRNA expression in a VZ subdomain of the MGE (Nery et al., 2001). In contrast, Shh transcripts were only faintly expressed in the cortex. Using RNAscope, whose sensitivity is higher than the sensitivity of standard ISH, we re-examined the expression pattern of *Shh* mRNA at E14.5. In the ventral forebrain, *Shh* transcripts detected by RNAscope showed the same pattern of expression as *Shh* transcripts detected by ISH (Fig.6A,B). In addition, the expression domains of *Shh* mRNAs and *Lhx-6* mRNAs, a cIN marker, overlapped in the mantle zone of the MGE (Fig.6A2). In the cortex, some cells oriented either radially in the VZ/SVZ or tangentially in the tangential migration pathways expressed *Shh* mRNAs at a very low level (1 or 2 dots versus large cluster for SHH(+) cells in the MGE) (Fig.6C1,C2). In the tangential migration streams where a large number of cIN expressed *Lhx-6* mRNAs (Fig.6C1,C2), cIN that co-expressed Lhx6 and Shh mRNAs represented only 4 to 6 % of cIN expressing Lhx6-transcript (Fig.6C3).

Antibodies that recognize the N-ter part of SHH [SHH-Nter, e.g. “activated” SHH) (Lee et al., 1994)] strongly labeled forebrain regions known to strongly express SHH (Kiecker and Lumsden, 2004; Loulier et al., 2005; Sahara et al., 2007), such aszona limitans intrathalamica at E12.5, lateral walls of the third ventricle and choroid plexus at E14.5 (Fig.S4), validating the SHH-Nter antibodies used here. At E14.5, SHH-Nter antibodies immunostained bright tiny dots aligned radially in the VZ/SVZ, and tangentialy in the IZ. In the CP, dots were again radially aligned and some CP cells presented a rather diffuse cytoplasmic staining, which was not observed in the bottom layers. (Fig.6D2). We observe no particular SHH enrichment in the lower IZ/SVZ where cIN migrate, suggesting that their contribution to the cortical pattern of SHH expression was minimal. Together, our ISH and immunostaining experiments show that the cortical SHH protein has probably an extrinsic origin as previously described at the early stage of cerebellum development (Huang et al, 2010).

Ontogeny of Kif7 mutant brain developmental defects.

After E14.5, the cortex of *Kif7* -/- embryos continued to develop. At E16.5, cIN continued to migrate tangentially and the deep stream of tangentially migrating cIN extended to the dorsal cortex in *Kif7* -/- embryos (Fig. S5A). Nevertheless, the tangential migration of cIN to the dorso-medial cortex remained delayed in *Kif7* -/- embryos, where cIN failed to reach the hippocampus at E16.5 despite the presence of TBR2(+) cells, which were observed in control brains (Fig.S5A). At E16.5, NG1a(+) thalamic axons reached the lateral cortex in both control and *Kif7* -/- brains. Nevertheless, thalamic axons were much less numerous in *Kif7* -/- than in control embryos and moreover exhibited abnormal trajectories within the cortical plate (Fig.S5B). Interestingly, cIN distributed abnormally within the *Kif7* -/- cortex at P0, showing an increased density in the upper cortical layers and a decreased density in the bottom layers, which were moreover thinner than in control brains, as illustrated by CTIP2(+) staining (Fig. S6). At this stage, the cortical trajectories of thalamic axons appeared even more aberrant in *Kif7* -/- brains: a dense bundle of NG1a(+) fibers ran below the cortical plate to the dorsal cortex and failed to invade the CP (Fig.S6).

DISCUSSION

Our aim in the present paper was to better understand the developmental origin of functional abnormalities (e.g. epilepsy, cognitive deficits, …) in cortical circuits of human patients with Kif7 mutations by characterizing developmental abnormalities of the cerebral cortex in a *Kif7* -/- mouse model. We show that *Kif7* ablation affected the development of the two populations of cortical neurons, cortical plate neurons and GABAergic interneurons, in specific and distinct ways, and in agreement with their dorsal and ventral telencephalic origin. Alterations of the CP development (lack of subplate cells in the dorsal cortex, and delayed corticofugal projection) was remiscient of defaults previously described in GLI3 null mutants that lack subplate neurons and pioneer cortical projections (Magnani et al., 2014). In contrast, the abnormal migration of *Kif7* -/- cIN in the developing cortex reflected the abnormal properties of the cortical layers on which cIN migrated (e.g. abnormal CXCL12 expression in the SVZ), as well as intrinsic migration defaults that mimicked the migratory defaults of wild type cIN treated with the SHH pathway inhibitor cyclopamine.
KIF7 ablation altered specifically and differently the SHH pathway activity in the both cortical cells subpopulations, in agreement with their dorsal or ventral origin.

Kif7 knock-out mice as a model to study the effect of mutation in the *KIF7* gene in human

The deletion of *Kif7* gene in mice led to lethality the first day of life, but up to birth, the brain developed and a previous study demonstrated that *Kif7* mutant mice was a good model to dissect the mechanism that led to corpus callosum agenesis in patients (Putoux et al., 2019). All patients carrying mutation in the KIF7 gene on both alleles have developmental delay/intellectual disability (ID) and some have seizures. Investigations on cerebral malformation by MRI have shown that some of them have alterations in the cerebral cortex including cortical atrophy (al-Gazali and Bakalinova, 1998; Ali et al., 2012; Walsh et al., 2013) and pachygyria (Tunovic et al., 2015). Detecting defects in the cerebral cortex is more demanding in MRI quality images that corpus callosum agenesis or molar tooth sign, we can speculate that the number of patients with cerebral cortex defects was underscored. Malformations of cortical development was recognized as causes of ID and epilepsy and the cellular defects underlying these pathologies could imply defects in cell proliferation, neuronal migration and differenciation that lead to improper excitatory/inhibitory balance, connectivity into the cortex or of cortex with other brain structures. The mechanism of action of KIF7 to transduce SHH ciliary dependent signaling has been debated. It has been accepted that SHH activates KIF7 binding to microtubules and its accumulation to the tip of the cilium, making the kinesin motor domain the most essential domain for SHH transduction. A more recent study proposed that KIF7 is an immobile kinesin translocated to the cilium tip after SHH binding by a complex KIF3A/Kif3B/KAP (Yue et al., 2022) suggesting that domains in the KIF7 gene essential to its function is more complex. This could explain why any mutation, even point mutation in the Coiled-coil domain or in C-terminal part of the KIF7 protein induces clinical feature as severe as when mutation led to a highly truncated protein. Another explanation is that any mutation causes unproper folding of the protein inducing its degradation by the proteasome.

KIF7 loss of function alters cortex organization and connectivity between the cortex and the thalamus

In mouse embryo, GLI3 plays a major role in the patterning of dorsal telencephalon and in the proliferation and differenciation of cortical neurons (Rallu et al., 2002; Wang et al., 2011; Wilson et al., 2012). The *Kif7* knock-down that likely decreases GLI3R level leads to a decrease of apical radial progenitors and basal IP divisions, and of neuronal differenciation (Guo et al., 2015). In fibroblast isolated from patient lung carrying KIF7 mutation and in E11.5 *Kif7* -/- whole embryo, the processing of GLI3-FL in GLI3-R is decreased and GLI-A increased leading to over-SHH signaling (Cheung et al., 2009; Putoux et al., 2011). Our study demonstrated that the level of GLI3-R was decreased in the developing cortex of the *Kif7* -/- embryons that show cortical defects including abnormal layering of principal neurons and sporadic heterotopia, and delayed connectivity between the cortex and the thalamus.

Heterotopia has been observed in one patient with two point mutations (each herited from one parent) in the Coiled-coil domain (Tunovic et al., 2015) and we found cortical heterotopia in some *Kif7* -/- brains. Heterotopia is not a landmark of ciliopathy but were detected in a Joubert syndrom patient carrying a mutation in the *CELSR2* gene coding for a planar cell polarity protein (Vilboux et al., 2017) essential for neural progenitor cell fate decision, neural migration, axon guidance and neural maturation (Boutin et al., 2012; Hakanen et al., 2022). The heterotopia observed in the patient and in the mice model are focal, it is possible that they were missed in other patients, however heterotopia further emphasized the mistrafficking of principal cells in KIF7 depleted brain. Disorganization of thalamo-cortical connectivity between has never been reported in patients with KIF7 mutation or generally in ciliopathic patients, thalamocortical connectivity is essential to cognitive performances in young infants (Alcauter et al., 2014) and its alteration leads to neurodevelopemental delay and later

life cognition (Jakab et al., 2020). Moreover, a link beween ciliary function, cortex development and connectivity with the thalamus has been shown previously in the mutant mice lacking planar cell polarity proteins CELSR2 and FZD3. These mice display ciliary defects and an abnormal development of tracts between the thalamus and the cortex leading to the hypotrophy of the intermediate zone, the layer containing TCA and corticofugal axons (Wang et al., 2002; Tissir et al., 2005).

Extra-cortical origine of SHH

The role of SHH in the cortex has been demonstrated however which cells synthetize the morphogen in this brain structure and how SHH protein is distributed has been controversial. Our data demonstrated a very low level of local *Shh* mRNA synthesis in the cortex at E14.5. In contrast,SHH protein is detectable throughout the cortex suggesting an extrinsic origin, for example from the cerebrospinal fluid. *Shh* mRNA is expressed in the choroid plexus of mice from E12 to E14.5 (Zakaria et al., 2019) and we found accordingly that SHH is present in the choroid plexus. SHH immunopositive dots observed in the cortex could be immobilized SHH bind to CDO/BOC co-receptor which are expressed in the developing cortex (data not shown), SHH/Patch complex internalized after the binding of the ligand or extracellular vesicles. This last hypothesis relies on data that have shown that SHH transport needs ESCRT-III member protein CHMP1A (Ibisler et al., 2015), SHH related proteins are found in exosomes secreted from Caenorhabditis elegans epiderman cells (He et al., 2014), Drosophila wing imaginal discs {Wang, 2002 #50}, chick notochord cells and human cell lines (Vyas et al., 2014). The long propagation of SHH has been evidenced in the Drosophila in the neuroaxis and paraxial structures, the developing tooth, the cartilage and the limb (Gritli-Linde et al., 2001) and in the limb bud of chick embryos within actin-based filopodia (Sanders et al., 2013). How SHH is transported thoughout the cortex should be further explored, however, it has already be shown that SHH as present in multivesicular bodies, in neurites and filipodia in the post natal hippocampus and cerebellum, and in hippocampal culture, moving SHH-immunolabeled vesicles are located inside and outside the cells (Eitan et al., 2016).

KIF7 deletion leads to defects in cortical interneurons migration

Analysis of the defects induced by genes mutated in ciliopathies focus mainly on principal cells that organize the cortical layer (Higginbotham et al., 2013; Hasenpusch-Theil et al., 2020). Cortical interneurons are born ventrally and migrate to the cortex during embryonic development. In this structure, the primary cilium of tangentially migrating cIN is functional and transduces local SHH signal that promotes cIN reorientation from tangential migratory streams toward the cortical plate (Baudoin et al., 2012). In the present study, SHH application on control cIN had a mild effect on migratory behaviors and increases the percentage of radially migrating cIN. Surprisingly, *Kif7* -/- cIN have an abnormal migratory behavior but that do not evoke a decreased inhibition (e.g; increased) of SHH signaling. On the contrary, *Kif7* -/- cIN show a migratory behavior very similar to cyclopamine treated control cIN in which SHH signaling is inhibited. By consequence, we propose that Kif7 -/- cIN which differentiate in a ventral telencephalic domain expressing high SHH level, present reduced Gli-A signaling, e.g. decreased SHH signaling. In addiction to this cell autonomous defect, Kif7 -/- cIN show defect in the ability to colonize the dorsal cortex, presumably caused by the decreased expression of CXCL12 (Tiveron et al., 2006; Lysko et al., 2011) in the dorsal suggesting an affect of the cortical substrate on cIN migration.

CONCLUSION

In summary, SHH signaling is essential for the migration of cortical interneurons according a cell autonomous mechanism. Moreover, using the *Kif7* -/- mice, we demonstrated that defects in cortical interneuron migratory behavior involves also a non cell autonomous mechanism as the cortical substrate was abnormal with thining of the cortex, mispositionning of cortical cell precursors and neurons and poor connectivity between the cortex and the thalamus. Patients carrying mutations in the KIF7 gene are classified as ciliopathic patients and display developmental delay leading to ID and epilepsy. We demonstrated using the murine model that these clinical feature could be caused by abnormal cellular distribution of excitatory and inhibitory neurons and presumably neuronal connectivity and/or excitatory/inhibitory balance in the cortex. Finally, by demonstrating focal heterotopia and disconnectivity between the cortex and the thalamus in the murine model, we hope to open a new field of clinical investigations using MRI and tractography to identify such defects in patients carrying mutations in the KIF7.

MATERIAL AND METHODS

Mice. E12.5 embryos to P0 neonates of the swiss and C57/Bl6J strains were obtained from pregnant females purchased at JanvierLabs (France). Wild type (WT) and *Kif7* KO animals expressing TdTomato in the MGE-derived cIN (Nkx2.1-Cre, Rosa26-TdTomato) were generated in our animal facility and mated to produce embryos. Kif7 +/- mice are a generous gift of Pr Chi-Chung Hui (the Provider, SickKids Hospital, Toronto, USA) and Prof Bénédicte Durand (the Transferor, CNRS, Lyon, France). The day of the vaginal plug was noted E0.5.

Immunohistochemistry. Heads of embryos were fixed by immersion in 0.1% picric acid /4% paraformaldehyde (PAF) in phosphate buffer (PB) for 4 hours and then in 4% PAF in PB overnight. After PBS washes, brains were dissected, included in 3% typeVII agarose and sectionned at 70 µm with a vibratome. Immunostaining was performed on free-floating sections as explain previously (Baudoin et al, 2012). Primary antibodies were goat anti SHH-Nter (1:100, R&D system AF464), goat anti Netrin G1a (NG1a) (1:100, R&D system AF1166), rabbit anti TBR1 (1:1000, Abcam ab31940), rabbit anti TBR2 (1:1000, Abcam ab23345), rabbit anti PAX6 (1:100, clone poly19013, Covance PRB-278P), rabbit anti GSH2 (1:2000, Millipore ABN162), chicken anti MAP2 (1:500, Novus, NB30213), and rat CTIP2 (1:1000, Abcam ab18465). Primary antibodies were incubated in PGT (PBS/gelatine 2g per L/TritonX-100 0.25%) with 0.1% glycine and 0.1% lysine for anti Netrin G1a antibodies and 3% BSA for anti SHH-Nter antibodies. Primary antibodies were revealed by immunofluorescence with the appropriate Alexa dye (Molecular Probes) or Cy3 (Jackson laboratories) conjugated secondary antibodies diluted in PGT (1:400). Bisbenzimide (1/5000 in PBT, Sigma) was used for nuclear counterstaining. Sections were mounted in mowiol/DABCO (25mg/mL) and imaged on a macroscope (MVX10 olympus) or an epifluorescence microscope (LEICA DM6000) using X 40 and X63 immersion objectives, or a confocal microscope (Leica TCS SP5) using a x40 objective. Merged images were acquired on the same section except for TBR1 with TBR2 aquired on adjacent sections. The fluorescence intensity along the depth of the cortex was assessed using the plot profile function of ImageJ under a 500 pixels wide line starting in the ventricle to the surface of the brain.

In situ hybridization. Specific antisense RNA probe for *Shh*, *Gli1* and *CxCl12* genes (gift of Marie-Catherine Tiveron) were used for in situ hybridization analyses. DIG-probes were synthesized with a labeling kit according to the manufacturer's instructions (Roche, France). *In situ* hybridization was performed according to a modification of (Tiveron et al., 1996) (see supplementary material). Sections were mounted on glass slides, dried, dehydrated in graded ethanol solutions, cleared in xylene and coverslipped with Eukitt.

RNAscop. Embryonic E14.5 heads were cuted in cold Leibovitz medium (Invitrogen) and immersion fixed in cold 4% (w/v) paraformaldehyde (PFA) in 0.12 m phosphate buffer, pH 7.4, overnight. Brains were then cryoprotected in PFA 4% /sucrose 10 %, embedded in gelatin 7.5% /sucrose10% at 4°C and frozen. Biological samples were kept at -80°C until coronally sectioned with the cryostat at 20 µm. RNAscope experiment was performed according manufacturer's instructions (RNAScope® Multiplex Fluorescent V2 Assay, ACDbio) after a pre-treatment to remove gelatin. Two different probes/channels were used (C1 for Shh, C2 for Lhx-6). Probes were diluted according manufacturer's instructions (1 Vol of C2 for 50 vol of C1) and dilution of the fluorophores (Opal 520 and 570) was 1:1500. Sections were mounted in mowiol/DABCO (25mg/mL) and imaged on a confocal microscop (Leica TCS SP5) using an immersion x10 or x63 objectives on 10 µm stacks of images (1 image /µm).

DiI experiments. Tiny crystals of DiI (1,1'-dioctadecyl-3,3,3'3'-tetramethylindocarbocyanine perchlorate) were inserted in the dorsal or lateral cortex of WT and KIF7 KO embryonic brains fixed at E14.5 by immersion in 4% PAF. Injected brains were stored in 4% PAF at room temperature in the dark for several weeks to allow DiI diffusion. Before sectioning, brains were included in 3% agar. Coronal sections 60 µm thick were prepared with a vibratome and collected individually in 4% PAF. Sections were imaged with a macroscope (MVX10 Olympus).

Whole brain clearing and imaging. E14 and E16 embryos were collected in cold L15 medium, perfused transcardially with 4% PAF using a binocular microscope. Brains were dissected and postfixed 3 days in 4% PAF at 4°C, and stored in PB at 4°C until clearing. Whole brain immunostaining and clearing was performed at RT under gentle shaking according to a modified version of the original protocol (Renier et al., 2016). Briefly, perfused brains were dehydrated in graded methanol solutions (Fischer Scientific) (20, 50, 80% in ddH_2O, 2x100%, 1h30 each), bleached overnight in 3% hydrogen peroxide (Sigma-Aldrich) in 100% methanol and rehydrated progressively. After PBS washes, brains were blocked and permeabilized 2 days in PBGT (0.2% gelatin (Merck), 0.5% triton X-100 (Sigma-Aldrich) in PBS). All buffer solutions were supplemented with 0.01% Sodium Azide (Sigma-Aldrich). Primary goat anti Netrin G1a (1:100, R&D system AF1166) and rabbit anti Tbr1 (1:1000, Abcam ab31940) and secondary (647 donkey anti-goat, Molecular probes, 1/1000) and cy3 donkey anti-rabbit, Jackson laboratories, 1/1000antibodies were diluted in PBGT solution containing 0.1% saponin (Sigma-Aldrich) and applied respectively 3 days and 1 day at 37°C, with 1 day of PBGT washes in between. Immunolabeled brains were washed 1 day in PBS, embedded into 1.5% low-melting agarose (Type VII, Sigma) in 1% ultra-pure Tris-acetate-EDTA solution, placed in 5-ml tubes (Eppendorf, 0030119452) and dehydrated 1h in each methanol baths (50%, 80% and 2x100%). Samples were then incubated for 3h in 33% methanol / 66% dichloromethane (DCM, Sigma-Aldrich), washed in 100% DCM (2x30 min) and incubated overnight (without shaking) in dibenzyl ether (DBE). Brains were stored in DBE at RT. Cleared samples were imaged on a light-sheet microscope (LaVision Biotec, x6.3 zoom magnification) equipped with a sCMOS camera (Andor Neo) and Imspector Microscope controller software. Imaris (Bitplane) was used for 3D reconstructions, snapshots and movies.

Brain slices. We dissected brains of E14.5 transgenic Nkx2.1-cre, TdTomato embryos in cold L15 medium, embedded in 3% type VII agar (Sigma, A0701) and sectioned coronally with a manual slicer as explained in Baudoin et al, 2012. Forebrain slices 250 µm thick were transferred in Millicell chambers and cultured for 4 hours in F12/DMEM medium supplemented with CFS 10% in a CO2 incubator (Merck Millipore) prior to pharmacological treatment and recording. Slices were incubated in drug for 2 hours before transfer in culture boxes equipped with a bottom glass coverslip for time-lapse imaging.

Pharmacological treatment. Either recombinant Mouse Shh (C25II), N-terminus (464-SH-025, R&D systems) at 0.5µg/mL final or cyclopamine (C4116, Sigma) at 2.5 µM final were added to the culture medium of slices and renewed after 12 hours. Recombinant Shh was reconstituted at 100 µg/mL in sterile PBS with BSA 0.1%. The stock solution of cyclopamine was 10 mM in DMSO and the culture medium of control experiments contained 1/4000 DMSO (vehicle). Control experiments in culture medium with and without vehicle did not differ and were analyzed together.

Videomicroscopy and image processing. Slices were imaged on an inverted microscope (Leica DMI4000) equipped with a spinning disk (Roper Scientific, USA) and a temperature-controlled chamber. Multi-position acquisition was performed with a Coolsnap HQ camera (Roper Scientific, USA) to allow the recording of the whole cortex. Images were acquired with a x20 objective (LX20, Fluotar, Leica, Germany) and a 561 nm laser (MAG Biosystems, Arizona). Z-stacks of 30 µm were acquired 50

µm away from the slice surface, with a step size of 2 µm and a time interval of 2 or 5 minutes for at least 21 hours. Acquisitions were controlled using the Metamorph software (Roper Scientific, USA). Cell trajectories were reconstructed on movies by tracking manually the cell rear with MTrakJ (ImageJ plugin, NIH, USA) and were clustered according to their position in cortical layers and to their orientation (see details in Fig.5). The migration speed of cells and the frequency and duration of pauses were extracted from tracking data using an excel macro.

Statistical analyses. All data were obtained from at least three independent experiments and are presented as mean ± SEM (standard error of mean). Statistical analyses were performed with the GraphPad Prism software or R. Statistical significance of the data was evaluated using the unpaired two-tailed *t* test, the Mann–Whitney test, the Chi2 test or the Two-way ANOVA test followed by a Bonferroni post-hoc test. Data distribution was tested for normality using the D'Agostino and Pearson omnibus normality test. Values of $p<0.05$ were considered significant. In figures, levels of significance were expressed by * for $p<0.05$, ** for $p<0.01$, *** for $p<0.001$ and **** for $p<0.0001$.

Study approval. Experiments have been validated and approved by the Ethical committee Charles Darwin (C2EA-05, authorized project 02241.02) and mice were housed and mated according to European guidelines.

Acknowledgements. This work was supported by Institut National de la Santé et de la Recherche Médicale (INSERM), Centre National de la Recherche Scientifique (CNRS), Sorbonne University. Agence Nationale de la Recherche (ANR, grant MIGRACIL to C.M.), Fondation pour la Recherche sur le Cerveau (grant R11080DD to C.M.), Fondation J. Lejeune (grant R14108DD to C.M.). Marie-Christine Tiveron is acknowledged for the gift of the CXCL12 expression vector. We thank all members of the Métin's Team for constructive discussions. We gratefully acknowledge the Imaging plateform facility of the Fer à Moulin Institute for the use of their microscopes, and the animal facility of the Fer à Moulin Institute for animal care and breeding.

We declare No Competing interests

Mutation	Domain lacking, truncated or mutation	Cerebral		Ref
		Clinical feature	Anatomical defects (cortical in bold)	
Hom c.67C>T, p.Arg33*	No kinesin motor and no Gli binding	DD/ID	Wide ventricles - Macrocephaly CC agenesis/hypoplasia - MTS	(1)
Hom c.233_234del, p.Leu78Profs*2	Truncated kinesin motor and no Gli binding	DD/ID	Macrocephaly- CC agenesis- MTS	(1)
Hom c.587dupT, p.Glu197Glyfs*19	Truncated kinesin motor, no Gli binding	DD/ID	Macrocephaly - CC agenesis	(1)
Hom c.687delG, p.Arg230Alafs*92	Truncated kinesin motor, no Gli binding	DD/ID	Wide ventricles – Macrocephaly - CC agenesis - **Poor frontal cortical development**	(1)
Hom c.217 delG, p.Ala73Profs*109	No Gli binding	DD/ID	CC agenesis/hypoplasia - MTS	(2)
Hom c.653_662del, p.218-221del	Deletion in kinesin motor	DD/ID	Wide ventricles – Macrocephaly - CC agenesis - **Cortical atrophy**	(3)
Hom c.1639_1640delinsT, p.Gly547Serfs*5	No Coiled-coil	DD/ID	Macrocephaly- MTS - CC agenesis/hypoplasia - **Temporal pachygyria**	(1)
Hom c.1643dupC, p.Arg549Alafs*40	No coiled-coil	DD/Mild ID	Macrocephaly - CC dysgenesis - Cerebellar hypotrophy	(4)
Hom c.1643dupC, p.Arg549Alafs*40	No coiled-coil	DD/Mild ID	Macrocephaly - CC agenesis - MTS	(4)
Hom c.2164G>T, p.Glu722*	No coiled-coil	DD/Mild ID	Macrocephaly	(4)
Hom c.2335G>T, p.Glu779 *	No Coiled-coil	DD/ID - Seizure	Macrocephaly - CC agenesis - Cerebellar hypoplasia - Abnormal formation of the brainstem	(5)
Hom c.2896_2897del	Deletion in Coiled-coil	DD/ID	CC dysgenesis	(6)
Hom c.3001C>T, p.Gln1001*	Truncated Coiled-coil	DD/ID	Wide ventricles – Macrocephaly - CC agenesis/hypoplasia- MTS	(1)
Hom c.529+2T>C	Mutation in kinesin motor	DD	MTS	(7)
c.2593-3C>G //c.3001C>T, p.Gln1001*	Mutation in Coiled-coil //Truncated Coiled-coil	ID	Macrocephaly - CC hypoplasia - MTS	(7)
c.1019dupT, p.Asn341Glnfs*122 // c.3331C>T, p.Arg1111*	Truncated kinesin motor and no Gli binding //Truncated Coiled-coil	DD	CC agenesis	(7)
Hom c2593 C>G //c3001C>T, p.? // p.Gln1001*	Mutation in Coiled-coil //Truncated Coiled-coil	DD/ID- Seizure	Macrocephaly - CC agenesis	(4)
Hom c.2272G>T	Mutation in Coiled-coil	DD/ID - Seizure	CC agenesis	(6)
Hom c.3179A >G	Mutation in Coiled-coil	DD/ Very mild ID	Macrocephaly – MTS - CC agenesis/hypoplasia - **Temporo-parietal atrophy**	(8,9)
c.461G>A // c.2959 G>A	Mutation in Coiled-coil	DD/ID - Seizure	Hydrocephalus - Cerebellar hypoplasia - CC agenesis/hypoplasia - **Pachygyria - Heterotopia**	(10)
c.3365C>G // c.2482G>A	Mutation in Coiled-coil	DD/ID - Seizure – Ataxia	CC agenesis/hypoplasia	(10)
Hom c2593-3 C>G	Mutation in Coiled-coil	DD/Mild ID	Macrocephaly - CC hypoplasy Large asymmetrical cisterna magna	(4)
Hom c.3331C>T	Mutation in Coiled-coil	DD/ID	CC agenesis - MTS	(6)

TABLE 1

References

al-Gazali LI, Bakalinova D (1998) Autosomal recessive syndrome of macrocephaly, multiple epiphyseal dysplasia and distinctive facial appearance. Clinical dysmorphology 7:177–184.

Alcauter S, Lin W, Smith JK, Short SJ, Goldman BD, Reznick JS, Gilmore JH, Gao W (2014) Development of thalamocortical connectivity during infancy and its cognitive correlations. The Journal of neuroscience : the official journal of the Society for Neuroscience 34:9067–9075.

Ali BR, Silhavy JL, Akawi NA, Gleeson JG, Al-Gazali L (2012) A mutation in KIF7 is responsible for the autosomal recessive syndrome of macrocephaly, multiple epiphyseal dysplasia and distinctive facial appearance. Orphanet journal of rare diseases 7:27.

Anvarian Z, Mykytyn K, Mukhopadhyay S, Pedersen LB, Christensen ST (2019) Cellular signalling by primary cilia in development, organ function and disease. Nat Rev Nephrol 15:199–219.

Asadollahi R et al. (2018) Clinical and experimental evidence suggest a link between KIF7 and C5orf42-related ciliopathies through Sonic Hedgehog signaling. European journal of human genetics : EJHG 26:197–209.

Bai CB, Joyner AL (2001) *Gli1* can rescue the in vivo function of *Gli2*. Development 128:5161–5172.

Barakeh D, Faqeih E, Anazi S, S. Al-Dosari M, Softah A, Albadr F, Hassan H, Alazami AM, Alkuraya FS (2015) The many faces of KIF7. Human genome variation 2:15006.

Baudoin JP, Viou L, Launay PS, Luccardini C, Espeso Gil S, Kiyasova V, Irinopoulou T, Alvarez C, Rio JP, Boudier T, Lechaire JP, Kessaris N, Spassky N, Metin C (2012) Tangentially migrating neurons assemble a primary cilium that promotes their reorientation to the cortical plate. Neuron 76:1108–1122.

Bellion A (2005) Nucleokinesis in Tangentially Migrating Neurons Comprises Two Alternating Phases: Forward Migration of the Golgi/Centrosome Associated with Centrosome Splitting and Myosin Contraction at the Rear. Journal of Neuroscience 25:5691–5699.

Boutin C, Goffinet AM, Tissir F (2012) Celsr1–3 Cadherins in PCP and Brain Development. In: Current Topics in Developmental Biology, pp 161–183. Elsevier. Available at: https://linkinghub.elsevier.com/retrieve/pii/B9780123945921000107 [Accessed December 4, 2023].

Braisted JE, Catalano SM, Stimac R, Kennedy TE, Tessier-Lavigne M, Shatz CJ, O'Leary DDM (2000) Netrin-1 Promotes Thalamic Axon Growth and Is Required for Proper Development of the Thalamocortical Projection. J Neurosci 20:5792–5801.

Bravo-Calderón DM, Assao A, Garcia NG, Coutinho-Camillo CM, Roffé M, Germano JN, Oliveira DT (2020) Beta adrenergic receptor activation inhibits oral cancer migration and invasiveness. Archives of Oral Biology 118:104865.

Chen J, Laclef C, Moncayo A, Snedecor ER, Yang N, Li L, Takemaru KI, Paus R, Schneider-Maunoury S, Clark RA (2015) The ciliopathy gene Rpgrip1l is essential for hair follicle development. The Journal of investigative dermatology 135:701–709.

Cheung HO, Zhang X, Ribeiro A, Mo R, Makino S, Puviindran V, Law KK, Briscoe J, Hui CC (2009) The kinesin protein Kif7 is a critical regulator of Gli transcription factors in mammalian hedgehog signaling. Science signaling 2:ra29.

Chiang C, Litingtung Y, Lee E, Young KE, Corden JL, Westphal H, Beachy PA (1996) Cyclopia and defective axial patterning in mice lacking Sonic hedgehog gene function. Nature 383:407–413.

Dafinger C, Liebau MC, Elsayed SM, Hellenbroich Y, Boltshauser E, Korenke GC, Fabretti F, Janecke AR, Ebermann I, Nurnberg G, Nurnberg P, Zentgraf H, Koerber F, Addicks K, Elsobky E, Benzing T, Schermer B, Bolz HJ (2011) Mutations in KIF7 link Joubert syndrome with Sonic Hedgehog signaling and microtubule dynamics. The Journal of clinical investigation 121:2662–2667.

Dahmane N, Sánchez P, Gitton Y, Palma V, Sun T, Beyna M, Weiner H, Ruiz i Altaba A (2001) The Sonic Hedgehog-Gli pathway regulates dorsal brain growth and tumorigenesis. Development 128:5201–5212.

Denaxa M, Chan C-H, Schachner M, Parnavelas JG, Karagogeos D (2001) The adhesion molecule TAG-1 mediates the migration of cortical interneurons from the ganglionic eminence along the corticofugal fiber system. Development 128:4635–4644.

Ding Q, Motoyama J, Gasca S, Mo R, Sasaki H, Rossant J, Hui C (1998) Diminished Sonic hedgehog signaling and lack of floor plate differentiation in *Gli2* mutant mice. Development 125:2533–2543.

Eitan E, Petralia RS, Wang YX, Indig FE, Mattson MP, Yao PJ (2016) Probing extracellular Sonic hedgehog in neurons. Biology open 5:1086–1092.

Endoh-Yamagami S, Evangelista M, Wilson D, Wen X, Theunissen JW, Phamluong K, Davis M, Scales SJ, Solloway MJ, de Sauvage FJ, Peterson AS (2009) The mammalian Cos2 homolog Kif7 plays an essential role in modulating Hh signal transduction during development. Current biology : CB 19:1320–1326.

Fotaki V, Yu T, Zaki PA, Mason JO, Price DJ (2006) Abnormal positioning of diencephalic cell types in neocortical tissue in the dorsal telencephalon of mice lacking functional Gli3. The Journal of neuroscience : the official journal of the Society for Neuroscience 26:9282–9292.

Gritli-Linde A, Lewis P, McMahon AP, Linde A (2001) The Whereabouts of a Morphogen: Direct Evidence for Short- and Graded Long-Range Activity of Hedgehog Signaling Peptides. Developmental Biology 236:364–386.

Guo J, Higginbotham H, Li J, Nichols J, Hirt J, Ghukasyan V, Anton ES (2015) Developmental disruptions underlying brain abnormalities in ciliopathies. Nature communications 6:7857.

Hakanen J, Parmentier N, Sommacal L, Garcia-Sanchez D, Aittaleb M, Vertommen D, Zhou L, Ruiz-Reig N, Tissir F (2022) The Celsr3-Kif2a axis directs neuronal migration in the postnatal brain. Progress in Neurobiology 208:102177.

Han Y, Wang B, Cho YS, Zhu J, Wu J, Chen Y, Jiang J (2019) Phosphorylation of Ci/Gli by Fused Family Kinases Promotes Hedgehog Signaling. Developmental Cell 50:610-626.e4.

Hasenpusch-Theil K, Laclef C, Colligan M, Fitzgerald E, Howe K, Carroll E, Abrams SR, Reiter JF, Schneider-Maunoury S, Theil T (2020) A transient role of the ciliary gene Inpp5e in controlling direct versus indirect neurogenesis in cortical development. eLife 9.

Hasenpusch-Theil K, Theil T (2021) The Multifaceted Roles of Primary Cilia in the Development of the Cerebral Cortex. Frontiers in cell and developmental biology 9:630161.

Hatanaka Y, Yamauchi K (2013) Excitatory Cortical Neurons with Multipolar Shape Establish Neuronal Polarity by Forming a Tangentially Oriented Axon in the Intermediate Zone. Cerebral Cortex 23:105–113.

Haycraft CJ, Banizs B, Aydin-Son Y, Zhang Q, Michaud EJ, Yoder BK (2005) Gli2 and Gli3 Localize to Cilia and Require the Intraflagellar Transport Protein Polaris for Processing and Function Barsh G, ed. PLoS Genet 1:e53.

He M, Subramanian R, Bangs F, Omelchenko T, Liem KF, Kapoor TM, Anderson KV (2014) The kinesin-4 protein Kif7 regulates mammalian Hedgehog signalling by organizing the cilium tip compartment. Nature cell biology 16:663–672.

Higginbotham H, Eom TY, Mariani LE, Bachleda A, Hirt J, Gukassyan V, Cusack CL, Lai C, Caspary T, Anton ES (2012) Arl13b in primary cilia regulates the migration and placement of interneurons in the developing cerebral cortex. Developmental cell 23:925–938.

Higginbotham H, Guo J, Yokota Y, Umberger NL, Su CY, Li J, Verma N, Hirt J, Ghukasyan V, Caspary T, Anton ES (2013) Arl13b-regulated cilia activities are essential for polarized radial glial scaffold formation. Nature neuroscience 16:1000–1007.

Hui C-C, Slusarski D, Platt KA, Holmgren R, Joyner AL (1994) Expression of Three Mouse Homologs of the Drosophila Segment Polarity Gene cubitus interruptus, Gli, Gli-2, and Gli-3, in Ectoderm- and Mesoderm-Derived Tissues Suggests Multiple Roles during Postimplantation Development. Developmental Biology 162:402–413.

Ibisler A, Hehr U, Barth A, Koch M, Epplen JT, Hoffjan S (2015) Novel KIF7 Mutation in a Tunisian Boy with Acrocallosal Syndrome: Case Report and Review of the Literature. Molecular syndromology 6:173–180.

Ingham PW, McMahon AP (2009) Hedgehog Signalling: Kif7 Is Not That Fishy After All. Current Biology 19:R729–R731.

Jakab A, Natalucci G, Koller B, Tuura R, Ruegger C, Hagmann C (2020) Mental development is associated with cortical connectivity of the ventral and nonspecific thalamus of preterm newborns. Brain and behavior 10:e01786.

Kiecker C, Lumsden A (2004) Hedgehog signaling from the ZLI regulates diencephalic regional identity. Nat Neurosci 7:1242–1249.

Kim C-W, Lee HK, Nam M-W, Lee G, Choi K-C (2022) The role of KiSS1 gene on the growth and migration of prostate cancer and the underlying molecular mechanisms. Life Sciences 310:121009.

Klejnot M, Kozielski F (2012) Structural insights into human Kif7, a kinesin involved in Hedgehog signalling. Acta crystallographica Section D, Biological crystallography 68:154–159.

Kohtz JD, Baker DP, Corte G, Fishell G (1998) Regionalization within the mammalian telencephalon is mediated by changes in responsiveness to Sonic Hedgehog. Development 125:5079–5089.

Komada M (2012) Sonic hedgehog signaling coordinates the proliferation and differentiation of neural stem/progenitor cells by regulating cell cycle kinetics during development of the neocortex. Congenital anomalies 52:72–77.

Komada M, Iguchi T, Takeda T, Ishibashi M, Sato M (2013) Smoothened controls cyclin D2 expression and regulates the generation of intermediate progenitors in the developing cortex. Neuroscience letters 547:87–91.

Komada M, Saitsu H, Kinboshi M, Miura T, Shiota K, Ishibashi M (2008) Hedgehog signaling is involved in development of the neocortex. Development 135:2717–2727.

Kon E, Cossard A, Jossin Y (2017) Neuronal Polarity in the Embryonic Mammalian Cerebral Cortex. Front Cell Neurosci 11:163.

Lee J, Ekker S, von Kessler D, Porter J, Sun B, Beachy P (1994) Autoproteolysis in hedgehog protein biogenesis. Science 266:1528–1537.

Li G, Adesnik H, Li J, Long J, Nicoll RA, Rubenstein JLR, Pleasure SJ (2008) Regional Distribution of Cortical Interneurons and Development of Inhibitory Tone Are Regulated by Cxcl12/Cxcr4 Signaling. J Neurosci 28:1085–1098.

Liem KF, He M, Ocbina PJR, Anderson KV (2009) Mouse Kif7/Costal2 is a cilia-associated protein that regulates Sonic hedgehog signaling. Proc Natl Acad Sci USA 106:13377–13382.

Loulier K, Ruat M, Traiffort E (2005) Analysis of hedgehog interacting protein in the brain and its expression in nitric oxide synthase-positive cells. Neuroreport 16:1959–1962.

Lysko DE, Putt M, Golden JA (2011) SDF1 regulates leading process branching and speed of migrating interneurons. The Journal of neuroscience : the official journal of the Society for Neuroscience 31:1739–1745.

Machold R, Hayashi S, Rutlin M, Muzumdar MD, Nery S, Corbin JG, Gritli-Linde A, Dellovade T, Porter JA, Rubin LL, Dudek H, McMahon AP, Fishell G (2003) Sonic Hedgehog Is Required for Progenitor Cell Maintenance in Telencephalic Stem Cell Niches. Neuron 39:937–950.

Magnani D, Hasenpusch-Theil K, Benadiba C, Yu T, Basson MA, Price DJ, Lebrand C, Theil T (2014) Gli3 controls corpus callosum formation by positioning midline guideposts during telencephalic patterning. Cereb Cortex 24:186–198.

Magnani D, Hasenpusch-Theil K, Jacobs EC, Campagnoni AT, Price DJ, Theil T (2010) The Gli3 hypomorphic mutation Pdn causes selective impairment in the growth, patterning, and axon guidance capability of the lateral ganglionic eminence. The Journal of neuroscience : the official journal of the Society for Neuroscience 30:13883–13894.

Maurya AK, Ben J, Zhao Z, Lee RT, Niah W, Ng AS, Iyu A, Yu W, Elworthy S, van Eeden FJ, Ingham PW (2013) Positive and negative regulation of Gli activity by Kif7 in the zebrafish embryo. PLoS genetics 9:e1003955.

Métin C, Godement P (1996) The Ganglionic Eminence May Be an Intermediate Target for Corticofugal and Thalamocortical Axons. J Neurosci 16:3219–3235.

Nery S, Wichterle H, Fishell G (2001) Sonic hedgehog contributes to oligodendrocyte specification in the mammalian forebrain. Development 128:527–540.

Niceta M, Dentici ML, Ciolfi A, Marini R, Barresi S, Lepri FR, Novelli A, Bertini E, Cappa M, Digilio MC, Dallapiccola B, Tartaglia M (2020) Co-occurrence of mutations in KIF7 and KIAA0556 in Joubert syndrome with ocular coloboma, pituitary malformation and growth hormone deficiency: a case report and literature review. BMC pediatrics 20:120.

Park HL, Bai C, Platt KA, Matise MP, Beeghly A, Hui C c., Nakashima M, Joyner AL (2000) Mouse *Gli1* mutants are viable but have defects in SHH signaling in combination with a *Gli2* mutation. Development 127:1593–1605.

Park SM, Jang HJ, Lee JH (2019) Roles of Primary Cilia in the Developing Brain. Front Cell Neurosci 13:218.

Pedersen LB, Akhmanova A (2014) Kif7 keeps cilia tips in shape. Nature cell biology 16:623–625.

Price DJ, Kennedy H, Dehay C, Zhou L, Mercier M, Jossin Y, Goffinet AM, Tissir F, Blakey D, Molnar Z (2006) The development of cortical connections. The European journal of neuroscience 23:910–920.

Putoux A et al. (2011) KIF7 mutations cause fetal hydrolethalus and acrocallosal syndromes. Nature genetics 43:601–606.

Putoux A et al. (2012) Novel KIF7 mutations extend the phenotypic spectrum of acrocallosal syndrome. Journal of medical genetics 49:713–720.

Putoux A, Baas D, Paschaki M, Morle L, Maire C, Attie-Bitach T, Thomas S, Durand B (2019) Altered GLI3 and FGF8 signaling underlies acrocallosal syndrome phenotypes in Kif7 depleted mice. Human molecular genetics 28:877–887.

Rallu M, Machold R, Gaiano N, Corbin JG, McMahon AP, Fishell G (2002) Dorsoventral patterning is established in the telencephalon of mutants lacking both Gli3 and Hedgehog signaling. Development 129:4963–4974.

Renier N, Adams EL, Kirst C, Wu Z, Azevedo R, Kohl J, Autry AE, Kadiri L, Umadevi Venkataraju K, Zhou Y, Wang VX, Tang CY, Olsen O, Dulac C, Osten P, Tessier-Lavigne M (2016) Mapping of Brain Activity by Automated Volume Analysis of Immediate Early Genes. Cell 165:1789–1802.

Sahara S, Kawakami Y, Izpisua Belmonte JC, O'Leary DD (2007) Sp8 exhibits reciprocal induction with Fgf8 but has an opposing effect on anterior-posterior cortical area patterning. Neural development 2:10.

Sanders TA, Llagostera E, Barna M (2013) Specialized filopodia direct long-range transport of SHH during vertebrate tissue patterning. Nature 497:628–632.

Shimamura K, Rubenstein JLR (1997) Inductive interactions direct early regionalization of the mouse forebrain. Development 124:2709–2718.

Sousa VH, Fishell G (2010) Sonic hedgehog functions through dynamic changes in temporal competence in the developing forebrain. Current Opinion in Genetics & Development 20:391–399.

Stumm RK, Zhou C, Ara T, Lazarini F, Dubois-Dalcq M, Nagasawa T, Höllt V, Schulz S (2003) CXCR4 Regulates Interneuron Migration in the Developing Neocortex. J Neurosci 23:5123–5130.

Tanaka D, Nakaya Y, Yanagawa Y, Obata K, Murakami F (2003) Multimodal tangential migration of neocortical GABAergic neurons independent of GPI-anchored proteins. Development 130:5803–5813.

Tissir F, Bar I, Jossin Y, De Backer O, Goffinet AM (2005) Protocadherin Celsr3 is crucial in axonal tract development. Nature neuroscience 8:451–457.

Tiveron M-C, Hirsch M-R, Brunet J-F (1996) The Expression Pattern of the Transcription Factor Phox2 Delineates Synaptic Pathways of the Autonomic Nervous System. J Neurosci 16:7649–7660.

Tiveron MC, Rossel M, Moepps B, Zhang YL, Seidenfaden R, Favor J, Konig N, Cremer H (2006) Molecular interaction between projection neuron precursors and invading interneurons via stromal-derived factor 1 (CXCL12)/CXCR4 signaling in the cortical subventricular zone/intermediate zone. The Journal of neuroscience : the official journal of the Society for Neuroscience 26:13273–13278.

Tole S, Ragsdale CW, Grove EA (2000) Dorsoventral Patterning of the Telencephalon Is Disrupted in the Mouse Mutant extra-toesJ. Developmental Biology 217:254–265.

Tunovic S, Baranano KW, Barkovich JA, Strober JB, Jamal L, Slavotinek AM (2015) Novel KIF7 missense substitutions in two patients presenting with multiple malformations and features of acrocallosal syndrome. American journal of medical genetics Part A 167A:2767–2776.

Vilboux T, Malicdan MC, Roney JC, Cullinane AR, Stephen J, Yildirimli D, Bryant J, Fischer R, Vemulapalli M, Mullikin JC, Steinbach PJ, Gahl WA, Gunay-Aygun M (2017) CELSR2, encoding a planar cell polarity protein, is a putative gene in Joubert syndrome with cortical heterotopia, microophthalmia, and growth hormone deficiency. American journal of medical genetics Part A 173:661–666.

Vyas N, Walvekar A, Tate D, Lakshmanan V, Bansal D, Cicero AL, Raposo G, Palakodeti D, Dhawan J (2014) Vertebrate Hedgehog is secreted on two types of extracellular vesicles with different signaling properties. Sci Rep 4:7357.

Walczak-Sztulpa J, Eggenschwiler J, Osborn D, Brown DA, Emma F, Klingenberg C, Hennekam RC, Torre G, Garshasbi M, Tzschach A, Szczepanska M, Krawczynski M, Zachwieja J, Zwolinska D, Beales PL, Ropers HH, Latos-Bielenska A, Kuss AW (2010) Cranioectodermal Dysplasia, Sensenbrenner syndrome, is a ciliopathy caused by mutations in the IFT122 gene. American journal of human genetics 86:949–956.

Walsh DM, Shalev SA, Simpson MA, Morgan NV, Gelman-Kohan Z, Chemke J, Trembath RC, Maher ER (2013) Acrocallosal syndrome: identification of a novel KIF7 mutation and evidence for oligogenic inheritance. European journal of medical genetics 56:39–42.

Wang H, Ge G, Uchida Y, Luu B, Ahn S (2011) *Gli3* Is Required for Maintenance and Fate Specification of Cortical Progenitors. J Neurosci 31:6440–6448.

Wang Y, Thekdi N, Smallwood PM, Macke JP, Nathans J (2002) Frizzled-3 is required for the development of major fiber tracts in the rostral CNS. The Journal of neuroscience : the official journal of the Society for Neuroscience 22:8563–8573.

Wilson SL, Wilson JP, Wang C, Wang B, McConnell SK (2012) Primary cilia and Gli3 activity regulate cerebral cortical size. Developmental Neurobiology 72:1196–1212.

Xu Q, Guo L, Moore H, Waclaw RR, Campbell K, Anderson SA (2010) Sonic Hedgehog Signaling Confers Ventral Telencephalic Progenitors with Distinct Cortical Interneuron Fates. Neuron 65:328–340.

Xu Q, Wonders CP, Anderson SA (2005) Sonic hedgehog maintains the identity of cortical interneuron progenitors in the ventral telencephalon. Development 132:4987–4998.

Yokota Y, Ghashghaei HT, Han C, Watson H, Campbell KJ, Anton ES (2007) Radial Glial Dependent and Independent Dynamics of Interneuronal Migration in the Developing Cerebral Cortex Chan-Ling T, ed. PLoS ONE 2:e794.

Yu W, Wang Y, McDonnell K, Stephen D, Bai CB (2009) Patterning of ventral telencephalon requires positive function of Gli transcription factors. Developmental Biology 334:264–275.

Yue Y, Engelke MF, Blasius TL, Verhey KJ (2022) Hedgehog-induced ciliary trafficking of kinesin-4 motor KIF7 requires intraflagellar transport but not KIF7's microtubule binding. Molecular biology of the cell 33:br1.

Zakaria M, Ferent J, Hristovska I, Laouarem Y, Zahaf A, Kassoussi A, Mayeur ME, Pascual O, Charron F, Traiffort E (2019) The Shh receptor Boc is important for myelin formation and repair. Development 146.

FIGURE LEGEND

Table 1. Clinical diagnosis of patients carrying mutation in the *KIF7* gene on both allele from the literature. The size of mutated proteins and which domain lacks or is mutated was calculated. Clinical features associated with cortical dysfunction is listed. Among cerebral defects, those observed in the cortex are enlighted. DD, developmental delay; ID, intellectual deficit; CC, corpus callosum; MTS, molar tooth sign.

Figure 1. The loss of KIF7 alters cortical anatomy at E14.5 without the loss of the boundary between the pallium and the subpallium in the lateral brain. *Kif7*-/- are microphtalmic (black arrow) and exhibit skin laxity (white arrow) (A). External examination of both faces of the brain reveals the thinning of the rostral telencephalon (black arrow) and the lack of olfactory tubercles (white arrows) (B). Anatomical defects of E14.5 *Kif7* -/- brain (C) investigated on coronal sections labeled with Hoescht (C1). The ventricles are enlarged (C2) and the cortical thickness is decreased (C3) in the mutant whereas brain width (C4) and heigth (C4) are normal. The boundary between the pallium and the subpallium in not altered in *Kif7* -/- lateral brain (D) with a restriction of the homeobox gene GSH2 in the ventricular layer of the ventral brain (D1) and TBR2 in the dorsal brain (cortex and hippocampus, D2). Graphs are representing mean and S.E.M. Data from 3 WT and 4 Kif7 -/- (with means of 3-4 values per animal). Data are analyzed by Two-way ANOVA or mixed model (GraphPad 8.1.0). For the ventricular surface and the cortex thickness, mix model reveals a genotype effect (C2 and C3, $p<0.0001$). Rostro-caudality effect was significant in brain width (C4, $p=0.0441$) and height (C5, $p=0.092$) with no effect on genotype. CX, cortex ; LGE, lateral ganglionic eminence ; MGE, median ganglionic eminence ; CGE, lateral ganglionic eminence ; PSB, pallium/subpallium boundary ; Th, thalamus. Scale bar, 250 µm.

Figure 2. Cortical alterations in mice lacking KIF7 at E14.5 visible on representative pictures of sections imaged on confocal microscop (A), epifluorescence microscop (B1) or macroscop (B2,C). The cortical plate and the subplate are abnormal in *Kif7* -/- as shown with TBR1 and MAP2 staining (A). The secondary progenitor layer is disorganized (B). TBR2(+) cells are less organized in the latero-dorsal axis in the mutant compared to WT with a switch toward the surface on the brain (B1). While TBR2 and TBR1 expressing cells are organized in separated layers in WT, these layers merge in the dorsal cortex in *Kif7* -/- (B2, white arrow). V, ventricle ; VZ, ventricular zone ; SVZ, subventricular zone ; IZ, intermediate zone ; MZ, marginal zone ; CP, cortical plate. Scale bar: 100 µm (A), 200 µm (B, C).

Figure 3. *Kif7* deletion disrupts of the connectivity between the cortex and the thalamus at E14.5. Corticofugal axons labeled by placement of DiI's crystal (red dots) in the dorsal and lateral cortex (A). After for 30 days, DiI labelling reveals a loss of projecting axons to the subpallium from the dorsal cortex in the mutant (A1) and less projection from the lateral cortex (A2) that never reach the thalamus and are lost in the ventral brain (white arrow, A3). Thalamo-cortical axons labeled with anti-Netrin G1a (NG1a) immunostaining do not reach the PSB in the mutant and are lost in the ventral brain (B, arrow). Whole-mount imaging of the brain immunostained with NG1a and TBR1 antibodies (C) reveals the lack of TCA projection to the cortex in the Kif7 -/- (white arrowheads) and an abnormal projection to the ventral brain (arrow, lateral view). CX, cortex ; LGE, lateral ganglionic eminence ; MGE, median ganglionic eminence ; PSB, pallium/subpallium boundary ; Th, thalamus; Hy, hypothalamus; IC, internal capsule; Vtel, ventral telencephalon. Scale bar: 250 µm.

Figure 4. The loss of KIF7 alters *Cxcl12* transcript expression and the distribution of cIN in Nkx2.1-Cre/R26R-Tomato mice brain at E14.5. *CxCl12* mRNA is expressed in the TBR2(+) layer and whereas expression in detectable up to the dorsal cortex in WT, it is expressed only up to the in *Kif7* -/- lateral cortex (A). Deep cIN migratory stream colocalized with outer intermediate progenitors [IP, TBR2(+)] and whereas cIN migrate to the dorsal cortex in WT, they stop in the *Kif7* -/- when IP layer switchs toward the surface of the brain (B) as shown on representative image (B1, right panel, white arrow) and on the quantification of the tangential migratory streams length from the entry to the pallium to the last detected cIN in the cortex [B2, graph represents the mean ± SEM; Two way ANOVA, statistical difference between layers (***, p=0.001) and genotype (*, p=0.0157) (WT, n=4 ; *Kif7* -/-, n=3)]. Deep and superfical cIN tangential migratory streams are closer in the *Kif7* -/- lateral cortex (C) as shown on macroscopic images of WT and *Kif7* -/- (C1) and represented on the graph showing the fluorescence along the ventricle/mz axis measured by plot profile (Fiji) along a line drawn from the ventricle to the surface of the cortex (C2). Scale bar: 200 µm.

Figure 5. Effect of the stimulation or blocking of SHH signaling pathway on cortical interneuron (cIN) migration. Representative image of the last frame of a movie in which cells were tracked in a Nkx2.1-Cre;Rosa26-TdTomato slice (control). Migratory behaviors of cIN are classified in clusters according their trajectories and in which layers they migrate: oblique migration in the VZ from and to the deep migration tangential stream (VZ, blue), tangential in the deep tangential stream (DS, red), radial and oblique to invade the CP (to CP, green), radial on long distances bidirectionally between the VZ and the MZ (LRR, pink), immobile or moving in a restricted volume in the deep migratory stream (dark red), VZ (dark blue) and CP (dark green), migrating to the ventral brain (orange) and migrating chaotically (tangentially out of migratory stream and with no directionality or layer specificity, gray). Number of cIN migrating tangentially in the superficial migratory stream (MZ) were not quantified as cells were too packed to be isolated individually (A). Graphs represent the percentage of cIN behaving in the

different migratory behaviors in E14.5 Nkx2.1-Cre;Rosa26-TdTomato brain slices *Kif7* -/- or untreated WT (control) or treated with cyclopamine (cyclo) or SHH (B). *Kif7* deletion and treatments with cyclopamine or affect cIN migratory behaviors compared to control conditions (Chi-square test, X^2 (24, N=3435), p<0.0001, ****). Schemes of experimental conditions enlighting how *Kif7* deletion and activation (SHH) or inhibition (cyclopamine) of SHH pathway affect cIN migration (C). Kinetics of moving cIN moving in the deep stream or to the cortical plate (D). Graphs represent the mean speed of cells (D1), the stop frequency (D2), the stop duration (D3). Krustkal-Wallis test in each cluster. ****, p<0.0001; ***, p<0.001; **, p<0.01; *, p>0.05 compared to control. VZ, ventricular zone ; SVZ, subventricular zone ; IZ, intermediate zone ; CP, cortical plate ; MZ ; marginal zone. Scale bar: 300 µm.

Figure 6. Expression of Shh mRNA and SHH-Nter protein in the developing cortex. Expression of *Shh* transcripts detected by *in situ* hybridization and RNAscope in median (A) and caudal (B) E14.5 brain sections. *In situ* hybridization of forebrain sections with an antisens *Shh* probes shows strong expression of *Shh* mRNA in the ventral forebrain [MGE and MGE/LGE/septum boundary (A1), CGE (B1)], in the zona limitans (ZLI) of dorsal thalamus and the border of the 3rd ventricle (B1). RNAscop of forebrain sections further confirmed the strong expression of *Shh* mRNA in the MGE/septum boundary that express *Lhx-6* mRNA (a transcription factor expressed in post-mitotic interneurons in the ventral brain) (A2) and the CGE (B2). At higher magnification, *Shh* mRNA fluorescence (in green) labels a subpopulation of interneuron cell bodies (in red) in the MGE/septum boundary, in the subventricular zone of the MGE and in more dispersed cells in the MGE mantle (A2) and in the lateral and dorsal cortex (arrows, C1 and C2). Among Shh mRNA expressing cells in the cortex, some are principal glutamatergic cells (arrowhead, C1) and only few cIN express the transcript (C3). The graph represents the mean ± SEM in the IZ-CP layers and MZ layer. Expression of SHH-Nter protein in E14.5 median brain sections (D). Representative images are captured with epifluorecence (D1) and confocal microscop (D2). Confocal images are a merged stacks of 10 images and enlargment of pictures are shown. SHH expression is detected in blood vessels and in brigth dots all over the cortical neuropile. At the PSB and in the lateral part of the LGE, SHH-Nter is detectable in brigth elements aligned along the ventricular/subventricular axis. CX, cortex ; LGE, MGE and CGE, lateral, medial and caudal ganglionic eminence, V3, third ventricle; ZLI, zona intra-thalamica; Th, thalamus; Hyp, hypothalamus; PSB, palium/subpallium boundary; VZ, ventricular zone; SVZ, subventricular zone; IZ, intermediate zone; CP, cortical plate; MZ, marginal zone. Scale bar: 500 µm (A, B, D1), 20 µm (C), 50 µm (D2).

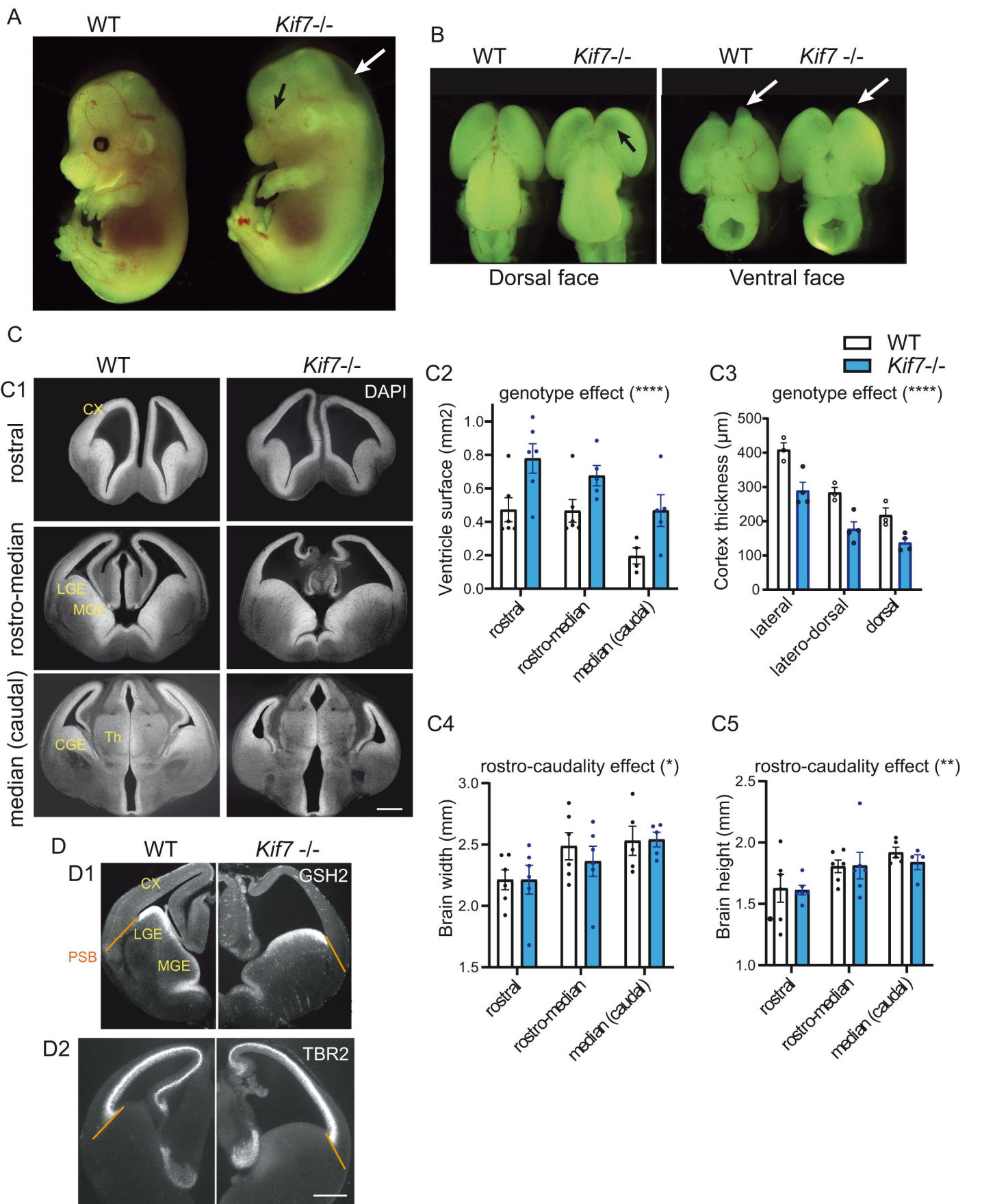
A
WT
Kif7-/-
B
WT
Kif7-/-
WT
Kif7 -/-
Dorsal face
Ventral face
C
WT
Kif7-/-
C1
DAPI
CX
rostral
LGE
MGE
rostro-median
CGE
Th
median (caudal)
C2
genotype effect (****)
Ventricle surface (mm2)
1.0
0.8
0.6
0.4
0.2
0.0
rostral
rostro-median
median (caudal)
C3
genotype effect (****)
Cortex thickness (µm)
500
400
300
200
100
0
lateral
latero-dorsal
dorsal
C4
rostro-caudality effect (*)
Brain width (mm)
3.0
2.5
2.0
1.5
rostral
rostro-median
median (caudal)
C5
rostro-caudality effect (**)
Brain height (mm)
2.5
2.0
1.5
1.0
rostral
rostro-median
median (caudal)
D
WT
Kif7 -/-
D1
CX
GSH2
LGE
PSB
MGE
D2
TBR2

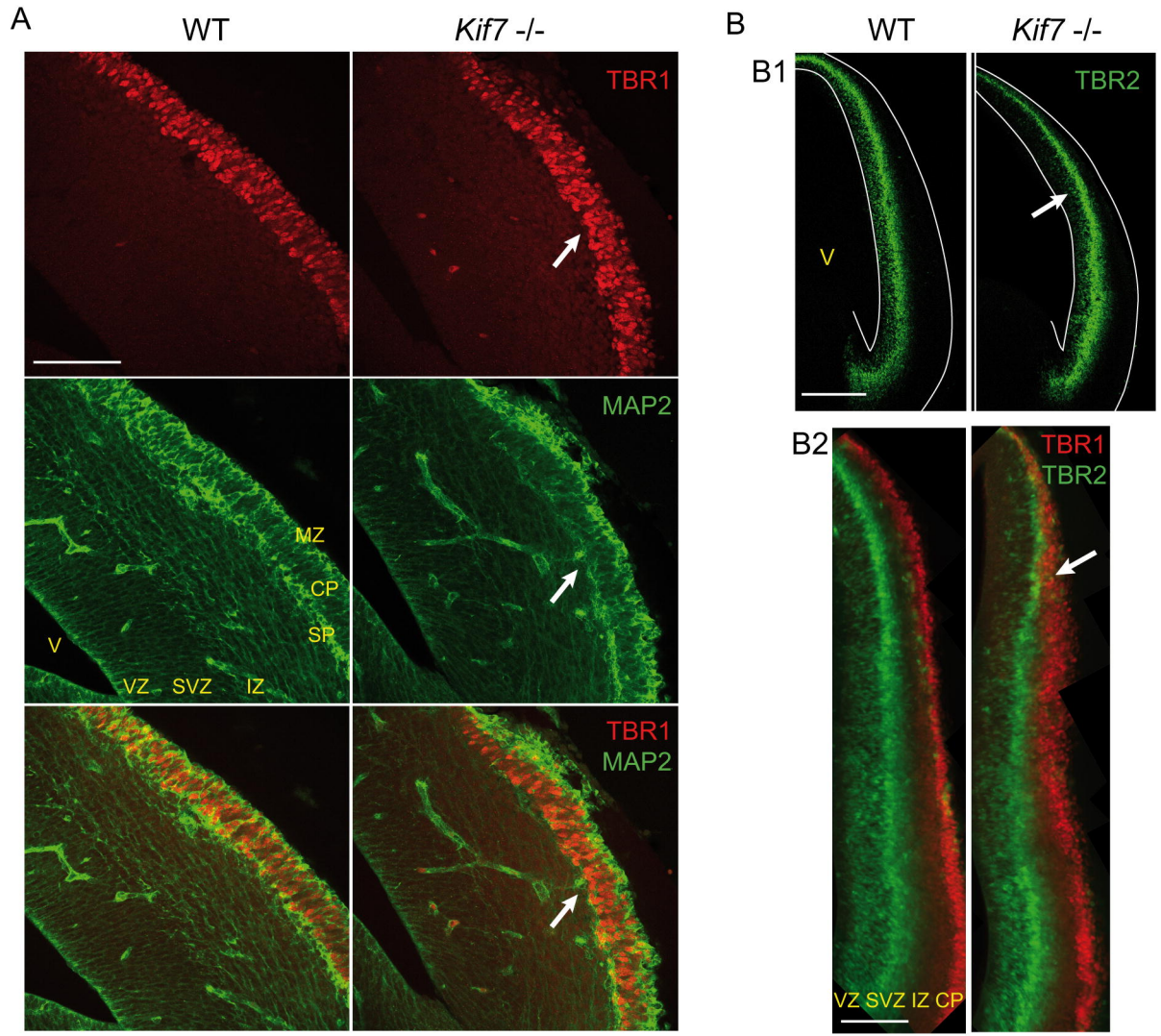
A
WT
Kif7 -/-
TBR1
MAP2
MZ
CP
SP
V
VZ
SVZ
IZ
TBR1
MAP2
B
WT
Kif7 -/-
B1
TBR2
V
B2
TBR1
TBR2
VZ SVZ IZ CP

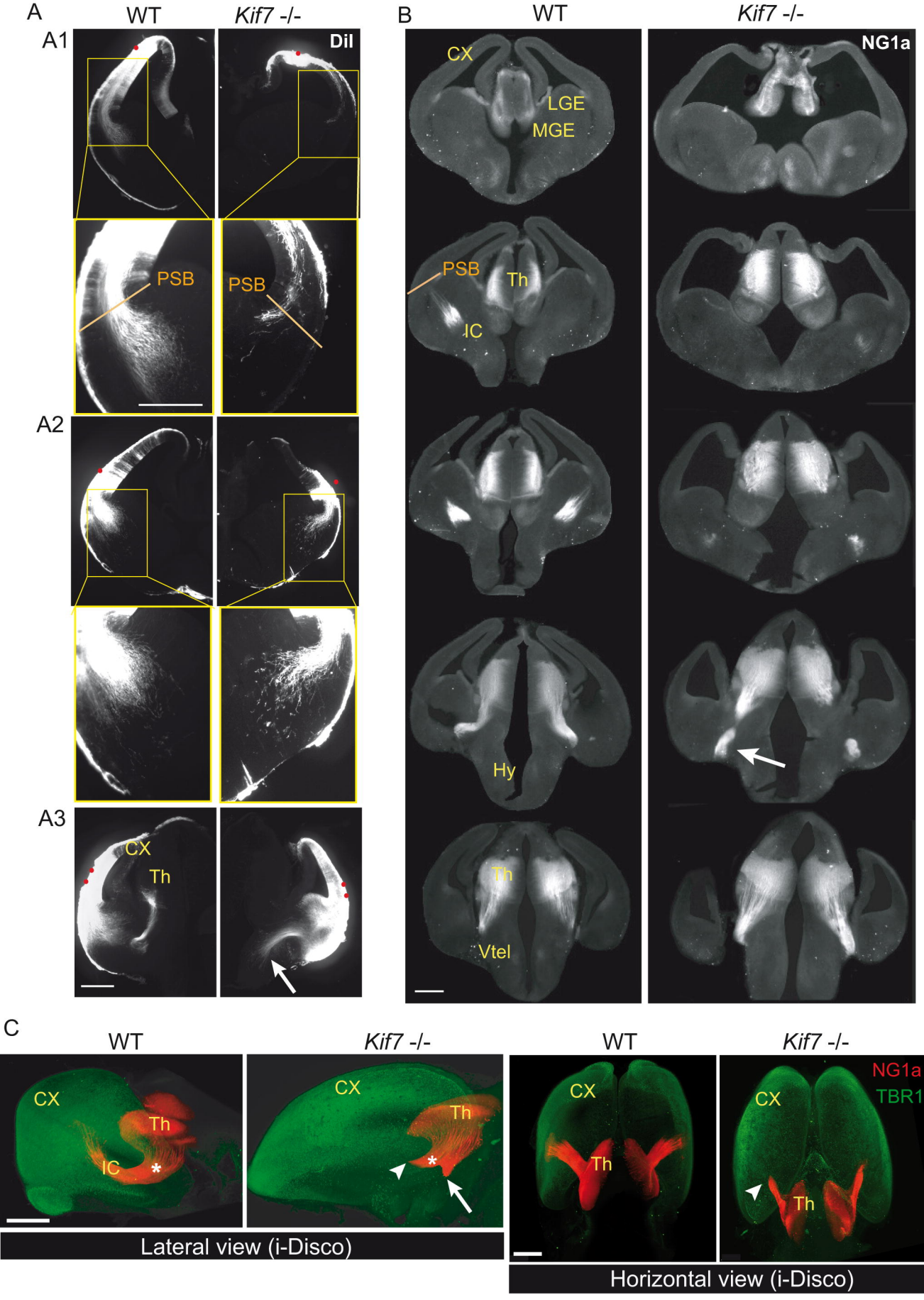
A
WT
Kif7 -/-
A1
DiI
PSB
PSB
A2
A3
CX
Th
B
WT
Kif7 -/-
NG1a
CX
LGE
MGE
PSB
Th
IC
Hy
Th
Vtel
C
WT
Kif7 -/-
CX
Th
IC
CX
Th
Lateral view (i-Disco)
WT
Kif7 -/-
NG1a
TBR1
CX
Th
CX
Th
Horizontal view (i-Disco)

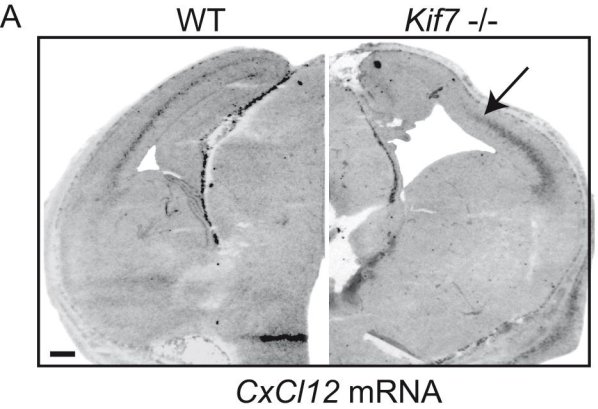
A
WT
Kif7 -/-
CxCl12 mRNA

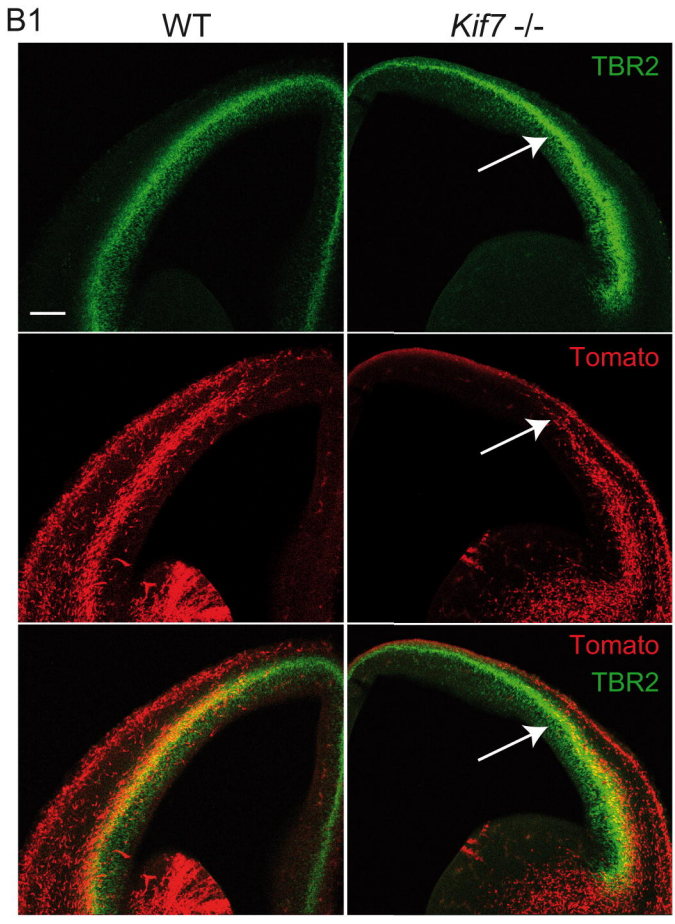
B
B1
WT
Kif7 -/-
TBR2
Tomato
Tomato
TBR2

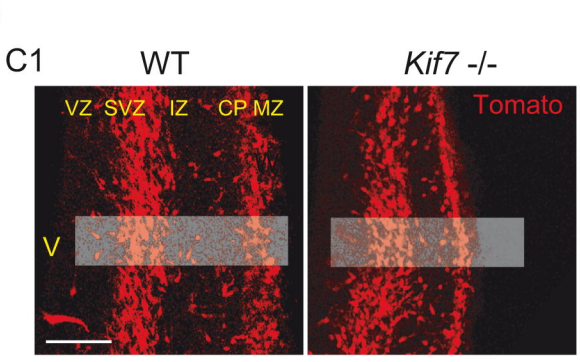
C
C1
WT
Kif7 -/-
VZ SVZ IZ CP MZ
V
Tomato

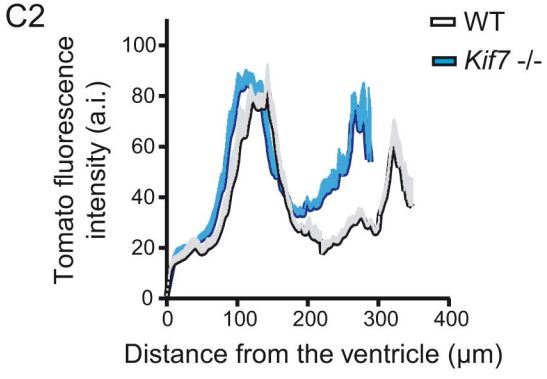
C2
WT
Kif7 -/-
Tomato fluorescence intensity (a.i.)
0
20
40
60
80
100
0
100
200
300
400
Distance from the ventricle (µm)

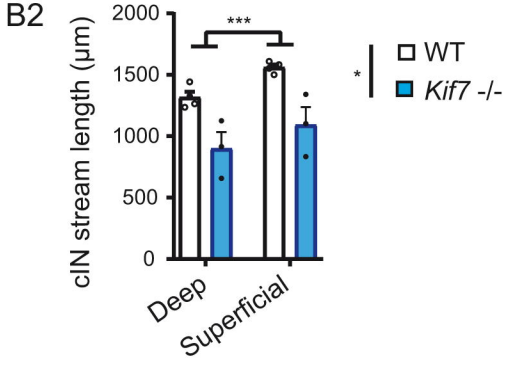
B2
cIN stream length (µm)
0
500
1000
1500
2000
***
*
WT
Kif7 -/-
Deep
Superficial

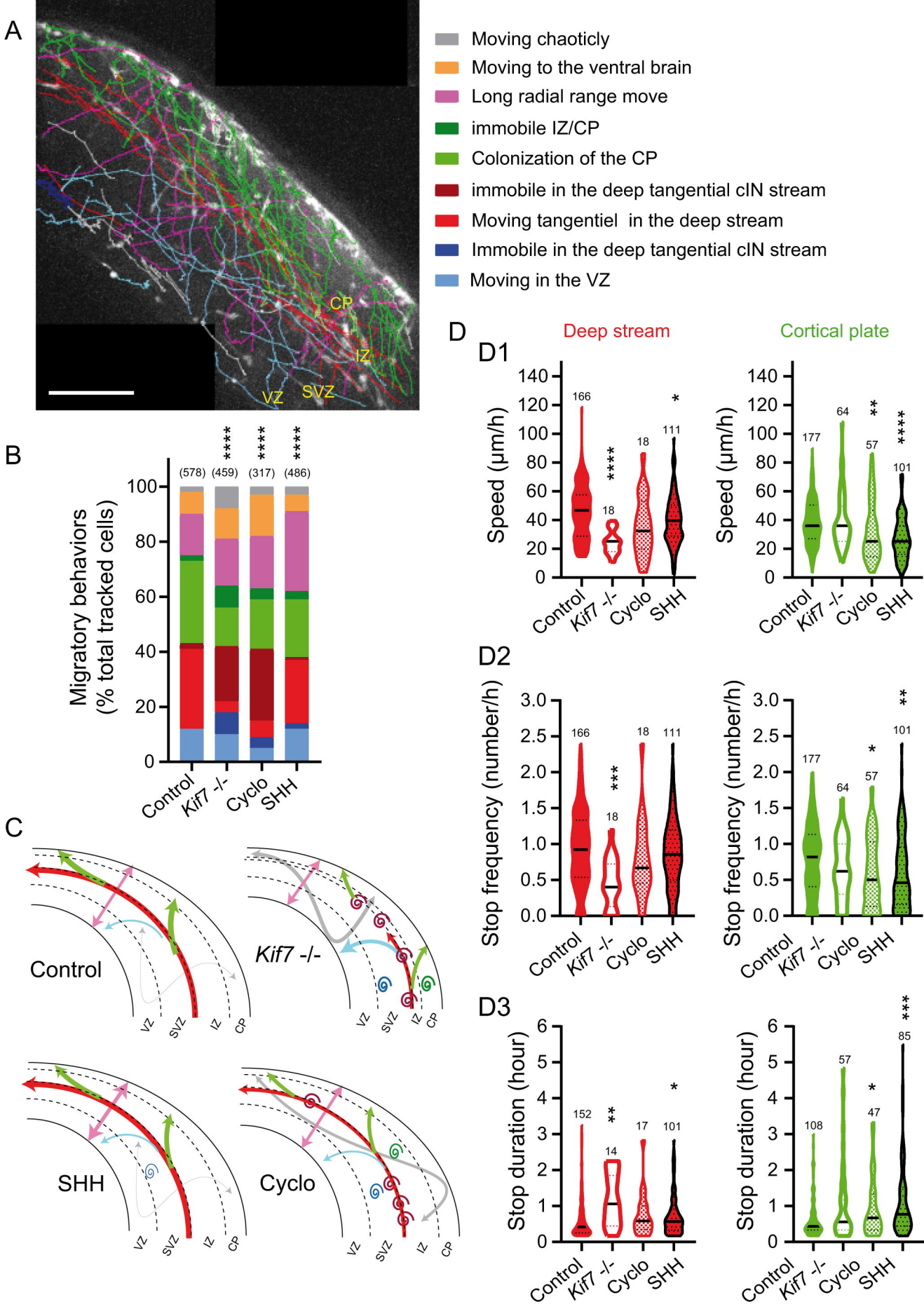
A
Moving chaoticly
Moving to the ventral brain
Long radial range move
immobile IZ/CP
Colonization of the CP
immobile in the deep tangential cIN stream
Moving tangentiel in the deep stream
Immobile in the deep tangential cIN stream
Moving in the VZ
CP
IZ
VZ
SVZ
B
Migratory behaviors (% total tracked cells)
(578)
(459)
(317)
(486)
****
Control
Kif7 -/-
Cyclo
SHH
C
Control
Kif7 -/-
SHH
Cyclo
VZ
SVZ
IZ
CP
D
Deep stream
Cortical plate
D1
Speed (µm/h)
D2
Stop frequency (number/h)
D3
Stop duration (hour)

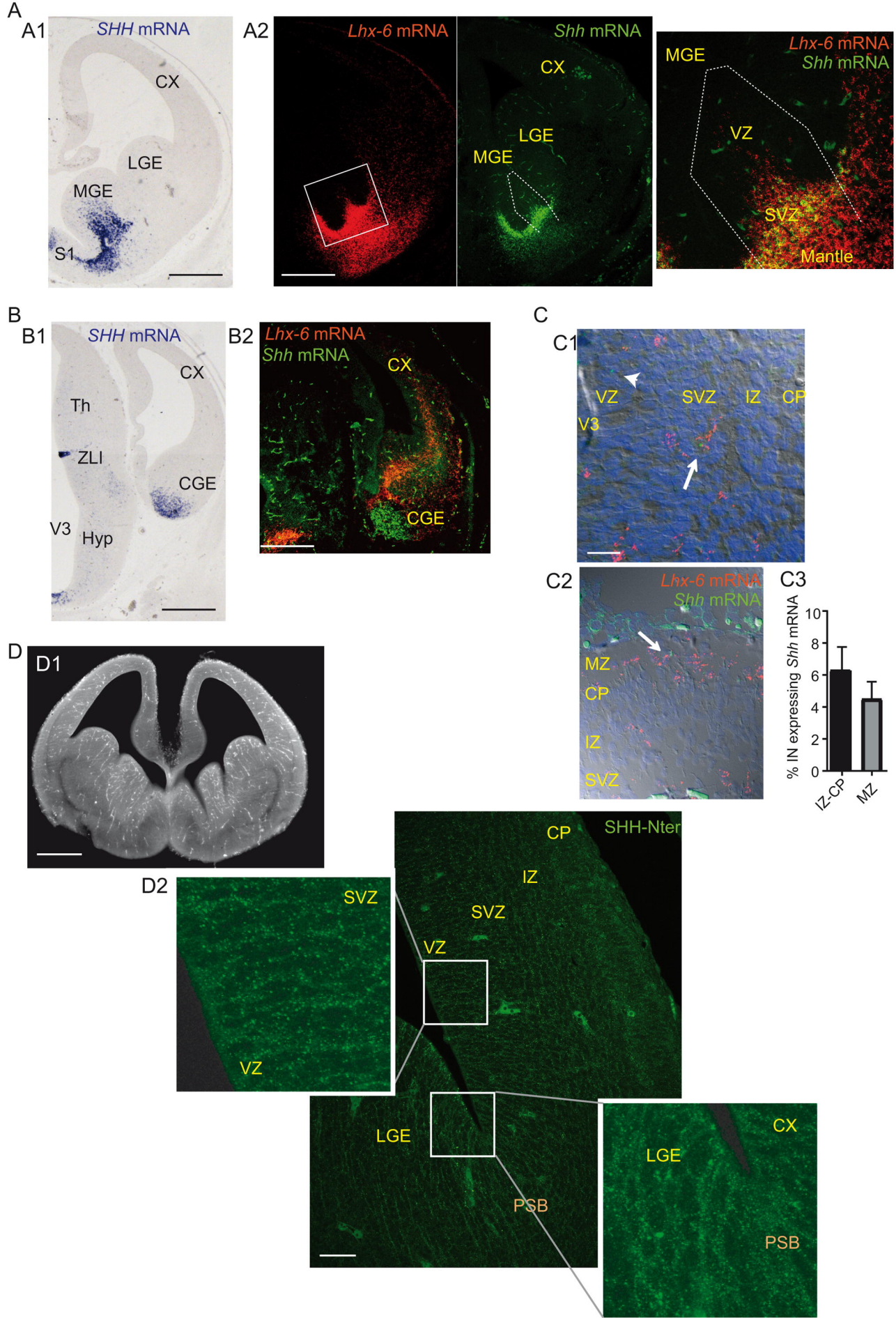
A
A1
SHH mRNA
CX
LGE
MGE
S1
A2
Lhx-6 mRNA
Shh mRNA
CX
LGE
MGE
MGE
Lhx-6 mRNA
Shh mRNA
VZ
SVZ
Mantle
B
B1
SHH mRNA
CX
Th
ZLI
CGE
V3
Hyp
B2
Lhx-6 mRNA
Shh mRNA
CX
CGE
C
C1
VZ
SVZ
IZ
CP
V3
C2
Lhx-6 mRNA
Shh mRNA
MZ
CP
IZ
SVZ
C3
% IN expressing Shh mRNA
10
8
6
4
2
0
IZ-CP
MZ
D
D1
D2
SVZ
VZ
CP
SHH-Nter
IZ
SVZ
VZ
LGE
PSB
CX
LGE
PSB